Studying Aerosol, Clouds, and Air Quality in the Coastal Urban Environment of Southeastern Texas

Michael P. Jensen,[a] James H. Flynn,[b] Jorge E. Gonzalez-Cruz,[c,d] Laura M. Judd,[e] Pavlos Kollias,[a,f] Chongai Kuang,[a] Greg M. McFarquhar,[g,h] Heath Powers,[i] Prathap Ramamurthy,[j] John Sullivan,[k] Allison C. Aiken,[i] Sergio L. Alvarez,[b] Peter Argay,[i] Brian Argrow,[l] Tyler M. Bell,[g,m] Doug Boyer,[n] Sarah D. Brooks,[o] Eric C. Bruning,[p] Kelcy Brunner,[p] Brian Butterworth,[q,r] Radiance Calmer,[r] Christopher D. Cappa,[s] Rajan K. Chakrabarty,[t] V. Chandrasekar,[u] Chun-Ying Chao,[v] Bo Chen,[o] Swarup China,[w] Don R. Collins,[x] Scott M. Collis,[y] Sean Crowell,[z] Rachael Dal Porto,[s] Gijs de Boer,[a] Min Deng,[a] Darielle Dexheimer,[1] Aryeh J. Drager,[a] Xuanlin Du,[x] Manvendra K. Dubey,[i] Andrew M. Dzambo,[h] Montana Etten-Bohm,[o] Jiwen Fan,[y] Ryan Farley,[s] Ya-Chien Feng,[w] Yan Feng,[y] Marta Fenn,[e] Richard E. Ferrare,[e] Samuel Flusche,[2] Ann M. Fridlind,[3] Joseph Galewsky,[4] Harold Gamarro,[j] Samuel Gardner,[p] Virendra P. Ghate,[y] Scott E. Giangrande,[a] Robert J. Griffin,[5] Travis Griggs,[b] Guillaume P. Gronoff,[e] Maxwell Grover,[y] Meghan Gaugenti,[6] Fangzhou Guo,[b,7] Siddhant Gupta,[y] Jiaxi Hu,[h,m] Yongjie Huang,[8] Robert C. Jackson,[y] Jonathan W. Hair,[e] Karen L. Johnson,[a] Sabin Kasparoglu,[9] Petra Klein,[h] Alexander E. Kotsakis,[k,10] Joshin Kumar,[t] Matthew R. Kumjian,[11] Katia Lamer,[a] Francesca M. Lappin,[h] Ziying Lei,[o] Jing Li,[t] Ron Li,[o] Yuezhi Li,[t] Timothy Logan,[o] Kelly Lombardo,[11] Edward P. Luke,[a] Zackary Mages,[f] Alyssa A. Matthews,[w] Brianna H. Matthews,[o] Olga Mayol-Bracero,[a] Toshihisa Matsui,[k,10] Katherine E. McKeown,[11] Manisha Mehra,[6] Fan Mei,[w] Nicholas Meskidzhe,[9] Cuong Nguyen,[12] Erik R. Nielsen,[o] Christopher J. Nowotarski,[o] David Oaks,[13] Rusen Oktem,[14] Mariko Oue,[f] Jungmin M. Park,[a] Nadia Partida,[b,i] Suarabh Patil,[g,h] Jean Carlos Pena,[d] Markus D. Petters,[x,9] Daniel B. Phoenix,[e] Joseph V. Puthserry,[t] Anita D. Rapp,[o] David M. Romps,[14] Maurice Roots,[k] Daniel Rosenfeld,[15] Stephen M. Saleeby,[u] Paul Savala,[2] Arthur J. Sedlacek,[a] Milind Sharma,[o] Rebeccca Sheesley,[6] Taylor J. Shingler,[e] Sujan Shrestha,[6] Ashish Singh,[a] Elizabeth N. Smith,[g,h] James N. Smith,[16] Scott Smith,[a] Jeffrey Snyder,[m] Elizabeth Spicer,[g,h] Elena Spinei,[k,17] Mark Spychala,[y] Philip Steir,[18] Michelle R. Storm,[g,h,m] Tamanna Subba,[a] B. Puigdomenech Treserras,[19] Rebecca Trojanowski,[a] Adam Theisen,[y] Seth A. Thompson,[o] Laurence Twigg,[k] Janek Uin,[a] Alexandra R. Ulinski,[b] Susan van den Heever,[u] Marcus van Lier-Walqui,[20,21] Adam C. Varble,[w] Timothy J. Wagner,[22] Jeremy Wakeen,[16] Nathan A. Wales,[i] Paul J. Walter,[2] Die Wang,[a] Jian Wang,[t] Lance Wood,[23] Yuxuan Wang,[b] Mengistu

Early Online Release: This preliminary version has been accepted for publication in *Bulletin of the American Meteorological Society*, may be fully cited, and has been assigned DOI 10.1175/BAMS-D-23-0331.1. The final typeset copyedited article will replace the EOR at the above DOI when it is published.

Wolde,[12] Subin Yoon,[b,24] Michael H. Young,[25] Maria A. Zawadowicz,[a] Qi Zhang,[26] Aifang Zhou,[a] Zeen Zhu,[a] Zihan Zhu[x]

[a] *Environmental Science and Technologies Department, Brookhaven National Laboratory, Upton, NY, USA*

[b] *Department of Earth and Atmospheric Sciences, University of Houston, Houston, TX, USA*

[c] *Atmospheric Sciences Research Center, University at Albany, Albany, NY, USA*

[d] *Department of Atmospheric and Environmental Science, University at Albany, Albany, NY, USA*

[e] *NASA Langley Research Center, Hampton, VA, USA*

[f] *School of Marine and Atmospheric Sciences, Stony Brook University, Stony Brook, NY, USA*

[g] *Cooperative Institute for Severe and High-Impact Weather Research and Operations, University of Oklahoma, Norman , OK, USA*

[h] *School of Meteorology, University of Oklahoma, Norman, OK, USA*

[i] *Los Alamos National Laboratory, Los Alamos, NY, USA*

[j] *Department of Mechanical Engineering, City College of New York, New York, NY, USA*

[k] *NASA Goddard Space Flight Center, Greenbelt, MD, USA*

[l] *Cooperative Institute for Research in Environmental Science, University of Colorado, Boulder, CO, USA*

[m] *NOAA/OAR National Severe Storms Laboratory, Norman, OK, USA*

[n] *Texas Commission on Environmental Quality, Austin, TX, USA*

[o] *Department of Atmospheric Sciences, Texas A&M University, College Station, TX, USA*

[p] *Department of Geosciences, Texas Tech University, Lubbock, TX, USA*

[q] *NOAA Physical Sciences Laboratory, Boulder, CO, USA*

[r] *Cooperative Institute for Research in Environmental Sciences, University of Colorado, Boulder, CO, USA*

[s] *Department of Civil and Environmental Engineering, University of California – Davis, Davis, CA, USA*

[t] *McKelvey School of Engineering, Washington University of St. Louis, St. Louis, MO, USA*

[u] *Colorado State University, Fort Collins, CO, USA*

[v] *Rice University, Houston, TX, USA*

[w] *Pacific Northwest National Laboratory, Richland, WA, USA*

[x] *Chemical and Environmental Engineering Department, University of California – Riverside, Riverside, CA, USA*

[y] *Argonne National Laboratory, Lemont, IL, USA*

[z] *LumenUs Scientific, LLC, Oklahoma City, OK, USA*

Accepted for publication in *Bulletin of the American Meteorological Society*. DOI 10.1175/BAMS-D-23-0331.1.

[1] *Sandia National Laboratories, Albuquerque, NM, USA*

[2] *Department of Mathematics, St. Edward's University, Austin, TX, USA*

[3] *NASA Goddard Institute of Space Studies, New York, NY, USA*

[4] *Department of Earth and Planetary Sciences, University of New Mexico, Albuquerque, NM, USA*

[5] *Roger Williams University, Bristol, RI, USA*

[6] *Environmental Sciences Department, Baylor University, Waco, TX, USA*

[7] *Aerodyne Research, Billerica, MA, USA*

[8] *Center for Analysis and Prediction of Storms, University of Oklahoma, Norman, OK, USA*

[9] *Department of Marine, Earth, and Atmospheric Sciences, North Carolina State University, Raleigh, NC, USA*

[10] *Earth System Science Interdisciplinary Center, University of Maryland, College Park, MD, USA*

[11] *Department of Meteorology and Atmospheric Sciences, Penn State University, University Park, PA, USA*

[12] *National Research Council of Canada, Ottawa, ON, Canada*

[13] *Hammelman Communications, Pagosa Springs, CO, USA*

[14] *Lawrence Berkely National Laboratory, Berkeley, CA, USA*

[15] *Hebrew University of Jerusalem, Mount Scopus, Jerusalem, Isreal*

[16] *Department of Chemistry, University of California – Irvine, Irvine, CA, USA*

[17] *Bradley Department of Electrical and Computer Engineering, Virgina Polytechnic Institute and State University, Blackburg, VA, USA*

[18] *Department of Physics, Oxford University, Oxford, England, United Kingdom*

[19] *McGill University, Montreal, Quebec, Canada*

[20] *Columbia University, New York, NY, USA*

[21] *Columbia University Center for Climate Systems Research at NASA GISS, New York, NY, USA*

[22] *Cooperative Institute for Meteorological Satellite Studies, Space Science and Engineering Center, University of Wisconsin, Madison, WI, USA*

[23] *National Weather Service Houston/Galveston Weather Forecast Office, League City, TX, USA*

[24] *Scripps Institute of Oceanography, La Jolla, CA, USA*

[25] *Jackson School of Geosciences, University of Texas at Austin, Austin, TX, USA*

[26] *Department of Environmental Toxicology, University of California - Davis, Davis, CA, USA*

Corresponding author: Michael P. Jensen, mjensen@bnl.gov

Accepted for publication in *Bulletin of the American Meteorological Society*. DOI 10.1175/BAMS-D-23-0331.1.

ABSTRACT

A multi-agency succession of field campaigns was conducted in southeastern Texas during July 2021 through October 2022 to study the complex interactions of aerosols, clouds and air pollution in the coastal urban environment. As part of the Tracking Aerosol Convection interactions Experiment (TRACER), the TRACER- Air Quality (TAQ) campaign the Experiment of Sea Breeze Convection, Aerosols, Precipitation and Environment (ESCAPE) and the Convective Cloud Urban Boundary Layer Experiment (CUBE), a combination of ground-based supersites and mobile laboratories, shipborne measurements and aircraft-based instrumentation were deployed. These diverse platforms collected high-resolution data to characterize the aerosol microphysics and chemistry, cloud and precipitation micro- and macro-physical properties, environmental thermodynamics and air quality-relevant constituents that are being used in follow-on analysis and modeling activities. We present the overall deployment setups, a summary of the campaign conditions and a sampling of early research results related to: (a) aerosol precursors in the urban environment, (b) influences of local meteorology on air pollution, (c) detailed observations of the sea breeze circulation, (d) retrieved supersaturation in convective updrafts, (e) characterizing the convective updraft lifecycle, (f) variability in lightning characteristics of convective storms and (g) urban influences on surface energy fluxes. The work concludes with discussion of future research activities highlighted by the TRACER model-intercomparison project to explore the representation of aerosol-convective interactions in high-resolution simulations.

SIGNIFICANCE STATEMENT

During 2021-2022 a series of field campaigns in Southeast Texas focused on studying the complex interactions of aerosols, clouds and air pollution in a coastal urban environment. This region, characterized by frequent clouds and storms, often driven by sea breezes, and diverse aerosol and pollution sources provides a unique setting to learn more about these interactions. The results presented here, and to follow from future research, will have important implications for coastal populations through improved understanding and prediction of the impacts of aerosols on the lifecycle of convective clouds, the influence of coastal circulation on air quality conditions, and the role that urban centers play in local weather.

CAPSULE

A succession of field campaigns conducted in Southeast Texas gathered data that is being used to study aerosol, cloud and air pollution interactions in a coastal urban environment.

Accepted for publication in *Bulletin of the American Meteorological Society*. DOI 10.1175/BAMS-D-23-0331.1.

1. Introduction

The complex environment of urban coastal regions presents significant challenges for our understanding of weather, climate, and air quality. Interactions between the land surface, water bodies, atmosphere, built environment, and anthropogenic forcings drive coupled processes that strongly influence the lifecycle of clouds, aerosol, and air quality. Southeast (SE) Texas offers a distinct humid subtropical environment to study these processes where summertime sea breeze (SB) circulations facilitate formation of isolated convective clouds that experience a spectrum of pollution conditions, ranging from high aerosol concentrations near the urban and industrial area of Houston-Galveston-Brazoria (HGB) to significantly lower aerosol concentrations in suburban and rural areas. Importantly, the HGB region is home to 7.1 million people as of 2020 (U.S. Census Bureau) and exhibits significant socio-economic diversity, leading to varied impacts from weather, climate and air quality factors.

The SE Texas region has a long history of atmospheric science field campaigns, particularly those focused on air quality and its evolution in the urban-coastal environment. The interrelated and overlapping field campaigns introduced in this paper build on the scientific outcomes of previous campaigns. In 2000, during the Texas Air Quality Study (TexAQS; Brock et al. 2003), aircraft measurements were collected with a goal of investigating the chemical and meteorological drivers of ozone air quality exceedances in the region. This was followed by the 2nd TexAQS in 2005-06 (Parrish et al. 2009), which expanded to consider regional sources and atmospheric processes that influenced ozone and aerosol formation and evolution in eastern Texas and the Gulf of America. The influence of these factors on large-scale radiative forcing and impacts on human health and regional haze were also important research targets. The 2009 Study of Houston Atmospheric Radical Precursors (Olaguer et al. 2014) aimed to resolve contributions of primary and secondary sources of important ozone precursors, formaldehyde and nitrous acid. With updated air quality regulations and a need to evaluate, improve and understand satellite-based retrievals, the Deriving Information on Surface Conditions from Column and VERtically Resolved Observations Relevant to Air Quality (DISCOVER-AQ; Bean et al. 2016, Yoon et al. 2021) campaign took place in several cities over multiple years, including a campaign over Houston in 2013. By collecting aircraft-based in situ and remote sensing observations over a network of surface-based sensors, DISCOVER-AQ focused on relationships between column-integrated and surface air quality variables towards improved interpretation of satellite-based measurements. During August and

Accepted for publication in *Bulletin of the American Meteorological Society.* DOI 10.1175/BAMS-D-23-0331.1.

September of 2013, concurrent with DISCOVER-AQ, the Studies of Emissions and Atmospheric Composition, Clouds and Climate Coupling by Regional Surveys (Toon et al. 2016) airborne field campaign was aimed at quantifying the role that deep convection plays in the vertical and regional distribution of pollutant emissions, gases, and aerosols. Following these campaigns, the processes contributing to high-ozone concentrations over Galveston Bay and offshore and how coastal circulations and other meteorological factors influence these and contribute to variability in pollutant concentrations over the southeast Texas region remains an area in need of further study and improved modeling.

SE Texas experiences a combination of significant populations of isolated convective clouds and diverse anthropogenic and natural aerosol sources. This prompted the Aerosol, Cloud, Precipitation and Climate (ACPC) initiative (https://acpcintiative.org) to target the region for exploring the interactions between aerosols and deep convection through a series of pilot projects. An analysis of multi-year observations from the Houston/Galveston (KHGX) NEXRAD shows that within 200 km, convection initiation (CI; $Z_e > 35$ dBZ) occurs 40-55 percent of the days over the annual cycle (Fridlind et al. 2019). They also reported strong peaks in the number of convective cells during the summer months of June through September. Hu et al. (2019) applied cell tracking to KHGX observations to investigate the lifecycle of isolated convective cells in varying aerosol conditions. They quantified regional variability in CCN number concentrations (N_{CCN}) from satellite observations following Rosenfeld et al. (2016). Hu et al. (2019) found that, for environments with surface-based convective available potential energy (CAPE) between 2000 and 4000 J kg^{-1}, there was an increase in maximum radar echo-top height and lightning mapping array source counts with increasing N_{CCN} up to 1000 cm^{-3}. Pehl et al. (2025) also examined KHGX data in combination with MERRA-2 data to show that deep convective clouds with higher aerosol loading had decreased warm rain, increased freezing, and increased vapor deposition onto ice.

To further investigate the influence of aerosols on deep convection, ACPC undertook a model intercomparison project (MIP; van den Heever et al. 2017, 2025). The ACPC MIP brought together eight state-of-the-art cloud-resolving models focused on the simulation of a case of scattered convective clouds in the SE Texas region. The goal was to characterize microphysical and dynamical responses of convective cloud populations to aerosol conditions and the robustness of these responses among the models. As summarized in Marinescu et al. (2021), there were many consistencies among the models' representation of convective

Accepted for publication in *Bulletin of the American Meteorological Society*. DOI 10.1175/BAMS-D-23-0331.1.

properties. There were similar changes in updraft speeds with high CCN concentrations, particularly for updrafts in the 4-7 km layer, where more frequent strengthening occurred. In the 5-8 km layer, there was notable drying of the updraft columns due to enhanced condensation and related water vapor depletion in the high CCN concentration simulations, dampening any impacts on the vertical velocity. However, important inconsistencies among the models were also identified. Most notably, there were differences in the number and/or sizes of convective updrafts and a large range of responses of the > 8 km updraft velocities from weakening to strengthening at these levels. Further, Saleeby et al. (2025) investigated deep convective cells simulated by the ACPC MIP models using the Tracking and Object Based Analysis of Clouds (*tobac)* cell identification and tracking algorithm (Heikenfeld et al. 2019a, b; Sokolowsky et al. 2024). The aerosol impacts on warm rain processes were found to be consistent among models over cell life cycles, while the aerosol response in the ice phase processes was highly variable among models and over cell lifetimes, thus suggesting greater variability and uncertainty in the ice phase parameterizations of the MIP models. The ACPC observational and modeling studies have highlighted the challenges to disentangling the complicated and often co-varying impacts of meteorology and aerosols on deep convective microphysics and dynamics (e.g. Varble et al. 2024).

Detailed WRF simulations with coupled Chemistry (WRF-Chem) of the ACPC MIP case and a fast spectral-bin microphysics scheme showed that the Houston urban heat island effect (UHI) may enhance the SB circulation and lead to quicker deepening of shallow warm clouds (Fan et al. 2020). The effects of anthropogenic aerosols become evident after the clouds became mixed phase, accelerating their development. Also, ACPC MIP simulations (Zhang et al. 2021) using the Morrison bulk microphysics scheme (Morrison et al. 2005, 2009; Morrison and Milbrandt 2011), showed that the commonly used saturation adjustment approach for condensation, which eliminates aerosol effects through supersaturation changes, diminishes aerosol invigoration of convection and precipitation; changing to an explicit representation of supersaturation for the condensation/evaporation calculation in the two-moment Morison scheme generated better agreement with both bin model results and with observations.

New field observations and early science results targeting the scientific uncertainties in aerosol, cloud, and air quality processes in the coastal urban environment of SE Texas region were recently undertaken and are summarized herein. The manuscript is organized as follows. First, the major interagency field campaigns' motivation and deployment strategies are

Accepted for publication in *Bulletin of the American Meteorological Society.* DOI 10.1175/BAMS-D-23-0331.1.

presented. This is followed by an overarching description of the conditions observed during the year-long campaign. A sampling of scientific results on aerosol lifecycle, air quality, SB circulations, cloud lifecycle, lighting and urban meteorology, are presented. Finally, plans for future research activities are presented.

2. Succession of Field Campaigns in Southeast Texas 2021-2022

From July 2021 through October 2022, a series of multi-agency field campaigns (Jensen et al. 2022) coordinated to collect a comprehensive set of observations in a complex urban-coastal environment to address fundamental questions at the intersection of meteorology, aerosol and cloud physics, and air quality. Collectively, we refer to the combined field campaigns as TRACER+. Originally, the multiple campaigns were intended to overlap during the summer of 2021, but due to varying agency travel restrictions, safety protocols, and requirements related to the SARS-CoV-2 COVID-19 pandemic, some campaign timelines needed to change, while others could not. The final campaign timelines are summarized in Figure 1c.

a. Tracking Aerosol Convection interactions ExpeRiment (TRACER)

The DOE's Atmospheric Radiation Measurement (ARM; Mather and Voyles 2013) facility supported TRACER (Jensen et al. 2023) from October 2021 through September 2022. The campaign was focused on quantifying the role that regional diversity of aerosol conditions plays in the evolution of the dynamical, microphysical, radiative, and electrification properties of isolated deep convective clouds. The main TRACER ground-based sampling site was located at the La Porte Municipal Airport in La Porte, TX [29.67°N, 95.06°W, 8 m] (Figure 1, Table S1). This site was selected as being a location that experiences substantial aerosol loading with diverse contributions from local anthropogenic sources (e.g., industry, agriculture, transportation), local natural sources (e.g., biogenic, marine aerosols) and long-range sources (e.g., biomass burning, Saharan dust). The ARM Mobile Facility (AMF1; Miller et al. 2016), with its full complement of cloud, aerosol, precipitation, meteorology, and radiation measurements (Tables S2-S3, Figures S1-S2), was deployed at this site for the full campaign with most instruments operating 24 hours per day, 7 days per week, offering a detailed look at the seasonal cycle.

An intensive operational period (IOP) was conducted during the months of June-September 2022 when an ARM ancillary (ANC) site was deployed in Guy, TX [29.33°N,

Accepted for publication in *Bulletin of the American Meteorological Society.* DOI 10.1175/BAMS-D-23-0331.1.

95.74°W, 20 m], southwest of Houston. This location was selected to represent a background rural site with less influence from urban impacts, particularly aerosol sources. A subset of meteorological and aerosol measurements (Table S2) was collected including detailed observations of aerosol size, number concentration, composition, and hygroscopicity. Also based at the ANC site, the Tethered Balloon System (TBS) conducted 149 flights during this IOP, to collect vertical profiles of aerosol and meteorological properties. Between these two ARM sites, a site at Pearland, TX [29.53°N, 95.28°W, 12 m] was selected to enable sampling by the 2nd generation C-band Scanning ARM Precipitation Radar (CSAPR2) over both the AMF1 and ANC sites with good sampling near the climatological summertime environmental 0°C level. The Multisensor Agile Adaptive Sampling (MAAS; Lamer et al. 2023) framework was employed to automatically identify and track isolated convective cells at high-resolution through their lifecycle. The three ARM sites are at similar distances from the Gulf coast (Figure 1) such that it was expected they would experience similar impacts from the SB circulation.

In addition to these baseline ARM sites, several sub-campaigns were added through the deployment of guest instrumentation (see complete list in Table S4). These campaigns helped to fill observational gaps, particularly in the regional and vertical variability of important aerosol and meteorological quantities. They also expanded the scientific scope to more explicitly include questions related to aerosol lifecycle, air quality, urban meteorology, and SB interactions.

b. NASA/TCEQ TRACER-Air Quality (TAQ)

TAQ (Judd et al. 2021) took place primarily during September 2021. Sponsored by NASA's Tropospheric Composition Research and Health and Air Quality Applied Sciences Programs and the Texas Commission on Environmental Quality (TCEQ), this synergistic effort was designed to measure air quality-relevant constituents at high spatial and temporal resolutions. Using instrument suites operated by NASA and collaborating institutions, TAQ combined ground-based supersites, mobile laboratories, and shipborne measurements with coincident overflights from an aircraft with remote sensing instrumentation. The goal of TAQ was to gain an updated understanding of the interactions among ozone photochemistry and local meteorology and provide observations to evaluate and improve-upon chemical transport models and satellite retrievals. A particular focus included preparation for NASA's first air quality geostationary satellite, Tropospheric Emissions: Monitoring of Pollution (TEMPO), which launched in Spring 2023 (Zoogman et al., 2017). TCEQ further supported additional air

Accepted for publication in *Bulletin of the American Meteorological Society.* DOI 10.1175/BAMS-D-23-0331.1.

quality observations from similar surface-based observational platforms during April-October 2022 (referred to as TAQ2), with an IOP in September 2022.

As part of TAQ during September 2021, the NASA Johnson Space Flight Center Gulfstream-V (G-V) had ten flight days, completing two or three raster patterns per day to measure air pollution over the Houston-Galveston region. These raster flight patterns are illustrated later in Figure 5. The G-V included instrumentation that made remote sensing measurements of column-integrated nitrogen dioxide (NO_2) and formaldehyde (HCHO) (Judd et al. 2019; Kowalewski and Janz 2014; Nowlan et al., 2018) and vertically resolved profiles of ozone and aerosols (Burton et al. 2012; Ferrare et al. 2023; Müller et al. 2014). Flights typically occurred on days when air quality forecasts predicted elevated concentrations of surface ozone in the afternoon. Ground-based platforms provided remotely sensed and in situ profiling of ozone (Sullivan et al. 2015; Young et al. 2017; Komhyr 1986; Smit and Thompson 2021), ozone precursors (NO2, HCHO; Herman et al. 2009) and aerosol (Welton et al. 2001). The TCEQ portion of TAQ included mobile air quality laboratories (Shrestha et al. 2023; Guagenti et al. 2025a), boat measurements (Griggs et al. 2024), and additional ozonesondes from on land and over the water. The 2022 TAQ2 campaign included similar mobile laboratory, boat, and balloon measurements with additional boat-based trace gas measurements and a small uncrewed aerial system (sUAS; Guagenti et al. 2025b). See the supplementary material for more details on TAQ/TAQ2 siting (Table S1) and instrumentation (Tables S5, S6).

c. Experiment of Sea Breeze Convection, Aerosols, Precipitation, and Environment (ESCAPE)

Towards improving predictability of convective clouds and related extreme weather events, the NSF-sponsored ESCAPE field campaign (Kollias et al. 2024) took place from 30 May to 30 September 2022. ESCAPE focused on the study of the coupling between convective cloud vertical motions, cloud and precipitation microphysics and precipitation production for varying environmental conditions, throughout the cloud lifecycle. From 31 May to 17 June 2022, the National Research Council (NRC) of Canada Convair-580 and the Stratton Park Engineering Company (SPEC) Learjet performed a combined 24 research flights (92 flight hours). Each aircraft was equipped with a comprehensive suite of remote-sensing and in situ instrumentation for measuring atmospheric state, aerosol, and cloud microphysics quantities. Flights were conducted over the Gulf, and east and west of the Houston city center. Due to a lack of deep convection during the campaign period, the sampling area was extended to include

Accepted for publication in *Bulletin of the American Meteorological Society.* DOI 10.1175/BAMS-D-23-0331.1.

flights over Lake Charles and Lafayette, LA. See Kollias et al. (2024) for more details on the ESCAPE flight paths, Dzambo et al. (2024) for more details on the forecasting and nowcasting operations, and Table S5 for a detailed list of ESCAPE aircraft instrumentation.

In addition to the aerial platforms, four ground-based mobile platforms were deployed during ESCAPE, three different mobile X-band radar systems (Pazmany et al. 2013; Cheong et al. 2013, Kollias et al. 2022 a,b), and a suite of boundary layer instrumentation on the Brookhaven National Laboratory Center for Multiscale Applied Sensing (CMAS) mobile laboratory (Lamer et al. 2022). Details on the ESCAPE surface mobile platforms are included in Table S6. The Colorado State University C-band Hydrological Instrument for Volumetric Observations (CHIVO) radar, employed the MAAS framework, operated from the AMF1 site from 1 August through 30 September 2022 (Kollias et al. 2023).

d. Convective Cloud Urban Boundary Layer Experiment (CUBE)

The NSF-sponsored CUBE took place during the June-September 2022 TRACER IOP. CUBE's primary objectives were to understand how urban boundary layer processes impact convection, and how urbanization impacts storm formation, movement, and dissipation in coastal urban regions (Rahman et al. 2024). As identified in Figure 1, CUBE deployed multiple field sites monitoring surface layer turbulence and boundary layer characteristics across a coastal-urban-rural transect including two urban locations (University of Houston – Moody Tower [UHMT], AMF1), one coastal site (University of Houston – Coastal Center [UHCC]), and a rural site northeast of Houston (Liberty, TX [LIB]).

e. Shared Campaign Weather Forecasting

To support operational decision-making during TAQ in September 2021 and the TRACER+ IOP in Summer 2022, a large ad hoc team of researchers, students, and professional forecasters met virtually to prepare and present a forecast of cloud, SB, and air quality conditions. This activity included a rotating team that included forecast coordinators who assembled forecasting teams, three forecasters who prepared and presented daily forecasts, and forecast assistants who gathered information and graphics. The forecast team used a combination of standard operational forecasting products, campaign-specific products (e.g., regional and local output from the GEOS-CF) and, real-time forecast runs from an enhanced version of the NASA-Unified WRF (NU-WRF; Peters-Lidard et al. 2015) to prepare the daily forecast. During the TRACER+ IOP, based on the forecast, a designated mission scientist decided for ARM

Accepted for publication in *Bulletin of the American Meteorological Society.* DOI 10.1175/BAMS-D-23-0331.1.

operations to remain in normal operations or move into enhanced operations (increasing radiosonde launch frequency and switching CSAPR2 to automated cell-tracking mode). Other TRACER, ESCAPE, TAQ, and CUBE research teams would then make independent decisions aligned with their own operational constraints and research objectives. A total of 40 enhanced operational days were conducted during the TRACER+ IOP (Figure S4).

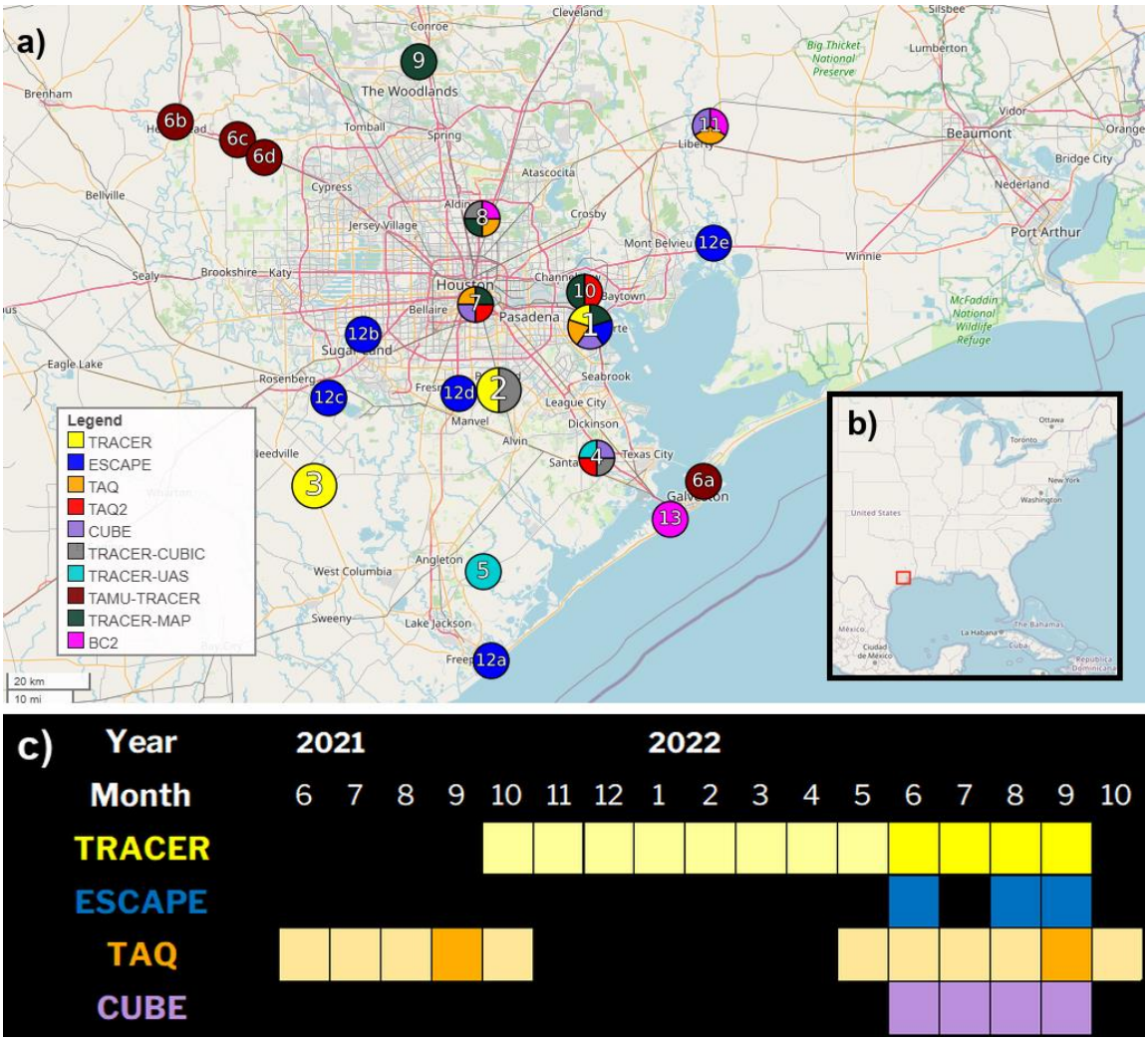

Fig. 1. a) Fig. 1. TRACER+ siting – [1] AMF1 – La Porte, [2] CSAPR2 site – Pearland, [3] ANC – Guy, [4] UHCC, [5] Brazoria sUAS flight locations, [6a] Galveston, [6b] Hempstead, [6c] Waller, [6d] Hockley, [7] University of Houston Launch Trailer (UHLT) and UHMT, [8] Aldine, [9] WG Jones State Forest, [10] San Jacinto Battleground, [11] Liberty (LIB) [12] Surfside and [13] Lake Charlotte. Site markers are color coded by campaign: TRACER (yellow), ESCAPE (blue), TAQ (orange), TAQ2 (red), CUBE (purple), TRACER-Coastal Urban Boundary Layer Interactions with Convection (CUBIC) (gray), TRACER-UAS (turquoise), Texas A&M University (TAMU)-TRACER (maroon), TRACER-Mapping Aerosol across Houston (MAP) (green), Texas Black Carbon – Brown Carbon (BC2) aerosol optical network (magenta). b) Inset showing the TRACER+ domain (red box). c) Schedule of TRACER+ interagency field campaigns. Highlighted colors represent IOPs.

3. Overall Campaign Conditions

Accepted for publication in *Bulletin of the American Meteorological Society.* DOI 10.1175/BAMS-D-23-0331.1.

The AMF1 instrumentation offered a detailed look at the seasonal cycle of cloud and aerosol properties, meteorological conditions, and radiative fluxes. These observations show distinct seasonal drivers of variability across SE Texas. Active remote sensing observations from the AMF1 are used to quantify the variability in cloud occurrence over the annual cycle. Figure 2a shows the vertical profile of cloud frequency of occurrence derived from the Active Remote Sensing of Clouds (ARSCL) value-added product (Clothiaux et al. 2000, 2001; Kollias et al. 2005, 2016). Isolated convection is seen throughout the TRACER campaign, with cloud tops frequently exceeding 15 km in late spring and throughout the summer. Stereo camera observations (Giangrande et al. 2023) confirm that convective clouds are more prevalent and, on average, deeper in summertime (Oktem 2021). Low-level clouds generally show lower cloud bases during the summer months consistent with a coupled boundary layer and moist surface layer (Figure 2a). Accumulated precipitation (Figure 2a) was notably low during the months of May, June and July with a significant increase in rainfall events and accumulation during August. The winter and fall months have noticeably higher precipitation amounts associated with frontal passages. Liquid water path (LWP; Figure 2c) increases steadily from the winter months through the spring, decreasing during the summer months minimums in the August, September, October time period.

Measurements from the ARM Aerosol Observing System (AOS; Uin et al. 2019) provide continuous in situ characterization of aerosol number concentration and size distribution, bulk chemical composition, sub- and super-saturated water uptake, radiative and optical properties, trace gas concentrations, and associated meteorological variables. Figure 3 shows the annual cycle of representative AOS measurements from the AMF1 site. A strong seasonal control on aerosol properties is observed. The summer months, when marine-influenced air masses with relatively higher rain rates, were most frequent, are generally cleaner than the winter, spring, and autumn months. Aerosol particles in the marine air masses during the summer are also associated with higher sulfate-to-organic ratios compared to the particles in continental air masses prevalent for the rest of the year (Fig. 3C). This is reflected in the particle sub-saturated (80% RH) hygroscopic growth factors shown in Figure 3D, which are higher in the summer, especially for particles > 50 nm. Kasparoglu et al. (2024b) show that aerosol hygroscopic properties strongly correlate with wind direction with southerly

Accepted for publication in *Bulletin of the American Meteorological Society*. DOI 10.1175/BAMS-D-23-0331.1.

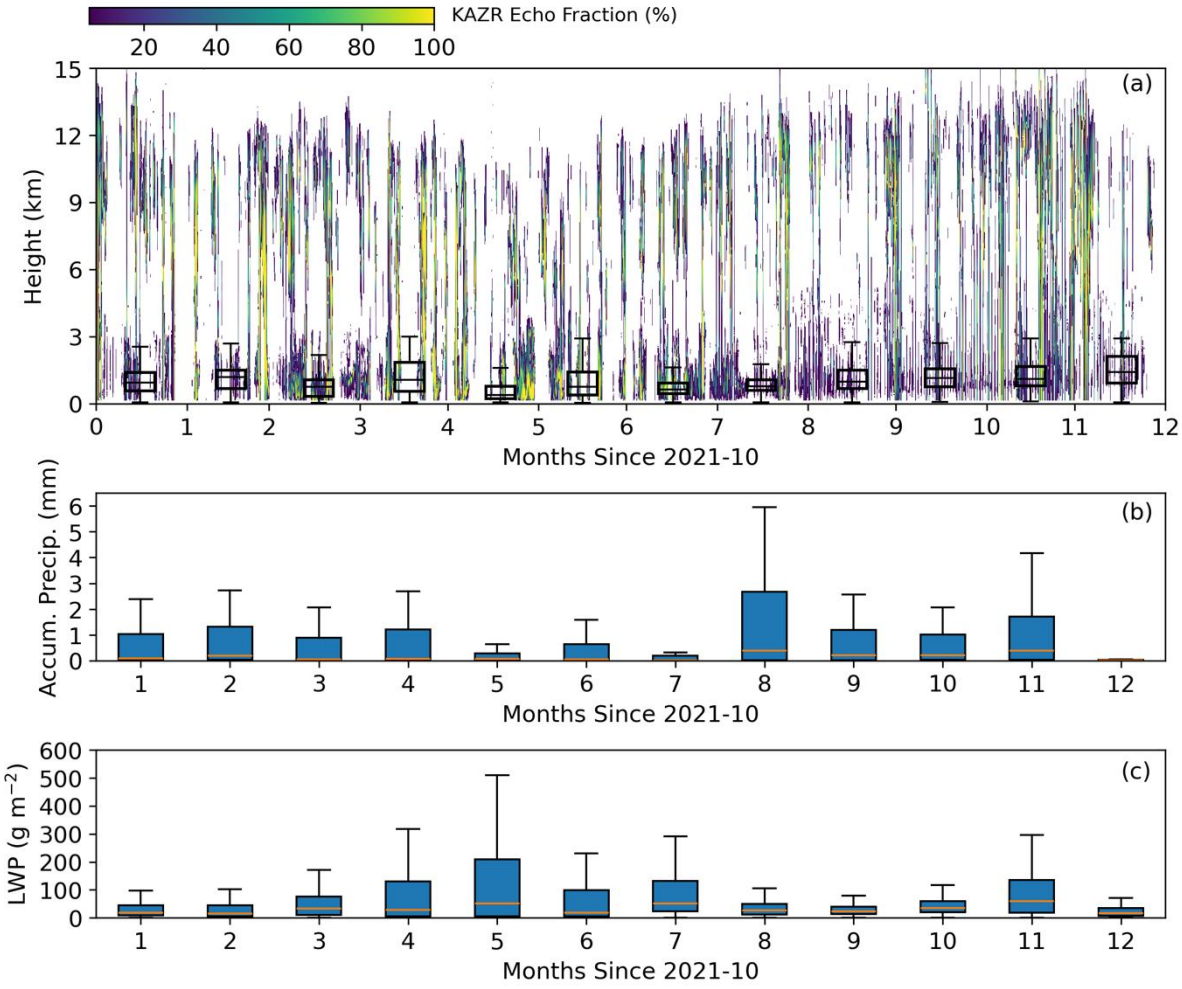

Fig. 2. Time series of cloud and precipitation properties at the AMF1 site over the full TRACER campaign (a) Ka-band ARM Zenith pointing Radar (KAZR) echo fraction over one-hour windows calculated from the ARSCL value-added product and monthly box and whisker plots (whisker show 90th and 10th percentile, boxes show 75th and 25th percentiles and line shows the median) of the ceilometer derived hourly cloud-base height for boundary layer clouds (cloud base height < 3 km), (b) hourly accumulated precipitation for each month and (c) hourly liquid water path derived from the microwave radiometer. For panel (a),radar transmitter issues limited radar sensitivity in September 2022, so profiles for that month likely underestimate cloud prevalence and vertical extent, as indicated by shading in the bottom panel (use with caution). For the box and whisker plots, zero values are not included.

Accepted for publication in *Bulletin of the American Meteorological Society.* DOI 10.1175/BAMS-D-23-0331.1.

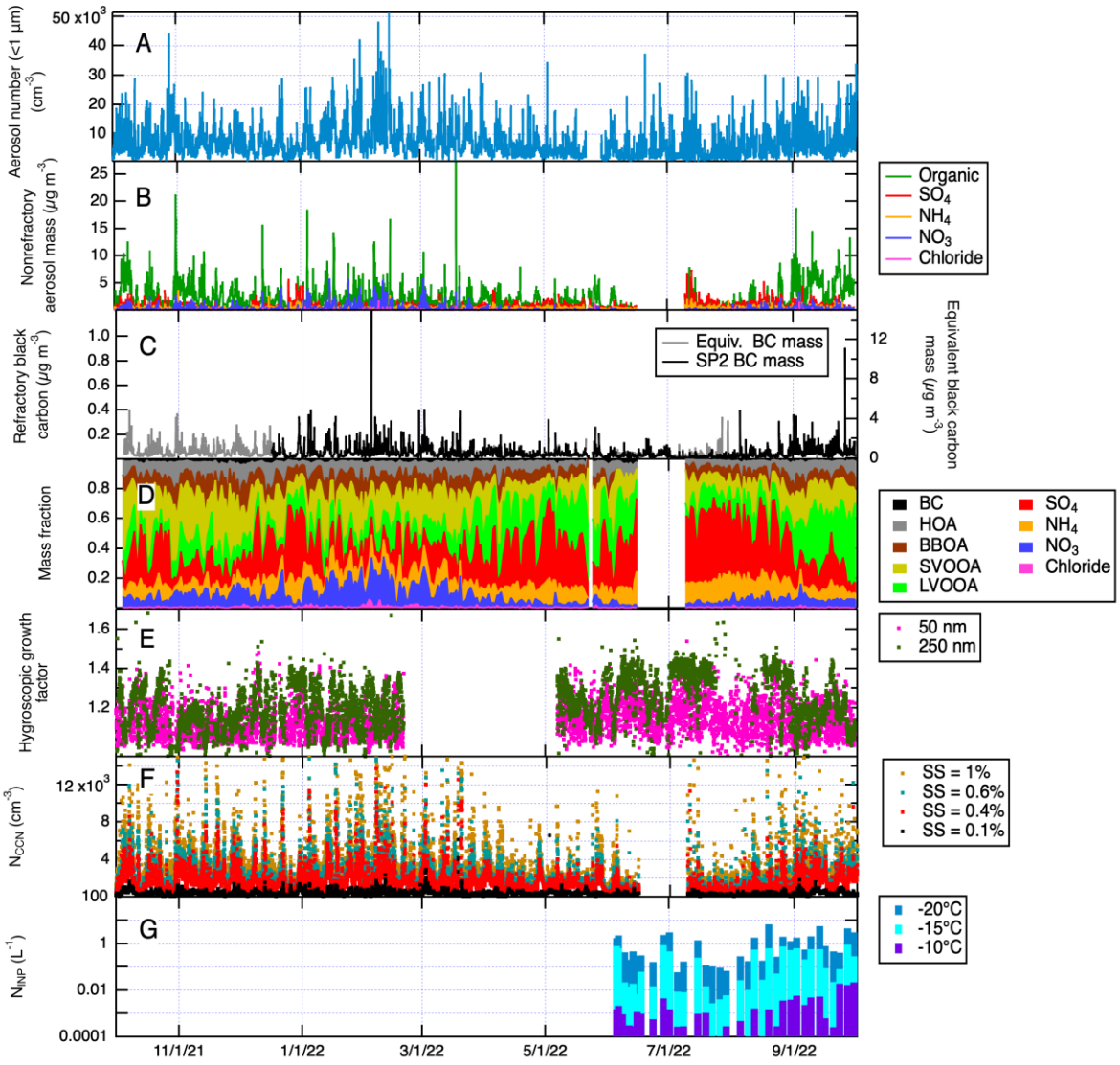

Fig. 3. Summary of observations from the ARM AOS deployed at the AMF1 site including: (A) Total concentration of submicron aerosol particles as measured by the Scanning Mobility Particle Sizer (SMPS), (B) aerosol composition derived from the Aerosol Chemical Speciation Monitor (ACSM), (C) refractory black carbon mass derived from the Single Particle Soot Photometer (SP2) and equivalent black carbon mass derived from the aethalometer, (D) speciated mass fractions from the ACSM, including organic source apportionment using positive matrix factorization, (E) size-resolved hygroscopic growth factor at 80% RH derived from the Humidified Tandem Differential Mobility Analyzer, (F) derived CCN concentrations at multiple supersaturations and (G) INP concentrations quantified off-line from filters collected at the AMF1 site. CCN concentrations were derived by calculating a bulk hygroscopicity parameter and from ACSM measurements to determine the critical diameter for each supersaturation. SMPS size distributions are then integrated for all sizes greater than the critical diameter.

flows bringing air from the Gulf featuring higher concentrations of hygroscopic particles. Derived CCN concentrations (Fig. 3E) also show a distinct seasonal cycle; however, despite higher hygroscopicity values in the summer, CCN concentrations are lower due to decreased total concentration of aerosols. In addition to particle composition and hygroscopicity, the

Accepted for publication in *Bulletin of the American Meteorological Society*. DOI 10.1175/BAMS-D-23-0331.1.

seasonal air mass origin also controls the concentration of ice-nucleating particles (INPs), which were collected at the main site during the IOP and measured off-line (Creamean et al., 2024). During the summer, marine air masses - identified through back-trajectory analysis (not shown) - are associated with lower concentrations of INPs than the typically polluted continental air masses.

To put the TRACER+ IOP (June-September 2022) in a climatological context, we investigate the large-scale synoptic regimes derived from a self-organizing map (SOM) analysis (Wang et al. 2022, 2024). We applied SOMs to thirteen summers (June-Sept.) 700-hPa geopotential height anomalies from the ERA5 (Hersbach et al. 2020) to characterize the dominant synoptic-scale regimes over SE Texas. Three dominant regimes emerged: (1) a pre-trough regime driven by the westward expansion of the Bermuda high, bringing substantial moisture to the region and favoring organized convection, (2) a post-trough regime with an upper-level low centered further inland to the north, resulting in cooler and drier conditions over SE Texas, and (3) an anticyclonic regime dominated by surface high pressure promoting the formation of SB circulations and the development of isolated convective clouds. Over the thirteen-year dataset, the pre-trough, post-trough, and anticyclonic regimes occurred 24%, 23% and 41% of the time, respectively. During the TRACER IOP period, the anticyclonic regime was even more frequent occurring on 64% of the IOP days, and the pre-trough and post-trough regimes occurred on 19% and 6% of the IOP days, respectively (Figure S5). Looking more closely at the synoptic-scale drivers of convection in the region, a climatology of CI in SE Texas for the month of June shows three distinct spatial patterns: CI only over land, CI only over the Gulf, and CI over both the land and Gulf (McKeown et al. 2025). For all CI regimes, there is a westward expansion of the Bermuda High and little synoptic forcing during the events. Only the land CI regime has coastal surface air temperature gradients supportive of SBs, indicating that other mesoscale ascent mechanisms are likely important. It is notable that the early weeks of the IOP were anomalously hot and dry, leading to record heat and lower-than-expected frequency of convective clouds (Kollias et al. 2025). This led to the scenario where the maritime side of the SB circulation often had more CAPE than the warmer continental side (e.g., Hanft and Houston 2018, Sharma et al. 2024).

4. A Sampling of Early Science Results from TRACER+

Accepted for publication in *Bulletin of the American Meteorological Society.* DOI 10.1175/BAMS-D-23-0331.1.

Here we highlight a few of the early science highlights, selected to represent the broad spectrum of TRACER+ research foci including aerosol lifecycle, convective cloud processes, air pollution and transport, the SB circulation, and urban-atmosphere interactions. We have chosen to feature unpublished results but conclude the section with a list of some published and additional TRACER+ results.

a. Aerosol Precursors in the Urban Environment

New particle formation (NPF) is an important aerosol source in both rural and urban environments and has been found to enhance the budget of CCN by ~2-4 times more in urban than rural regions (Ren et al. 2021). Specialized instrumentation was deployed from July 1st to August 31st, 2022, to investigate the frequency of NPF and the mechanisms by which particles formed and grew. During this period, Thermal Desorption Chemical Ionization Mass Spectrometry (TDCIMS; Voisin et al. 2003; Smith et al. 2004) was used to measure the size-resolved chemical composition of ultrafine particles in the urban environment. Overall, six NPF events were observed through July and August. We highlight a time during July 2022, where two distinct periods were observed: an "active" period during 8-16 July characterized by high concentrations of ultrafine (sub-100 nm diameter) particles with two NPF events and an "inactive" period with no observable NPF events during 17-23 July. The active period experienced elevated levels of ozone, exceeding 100 ppb most days, while the inactive period was typically below 60 ppb. Additionally, the inactive period contained multiple cloudy days and thunderstorms, which led to a decrease in total solar radiation compared to the active period. Figure 4 shows distinctly different chemical compounds associated with an active-period NPF event on 10 July compared to particles sampled during an inactive day (21 July). The event on 10 July was influenced by winds predominantly from the southwest, while the inactive day was influenced by winds directly from the south with higher humidity than the NPF event. The NPF event was characterized by detection of 12-nm diameter particles (the detection limit of the SMPS) and an average growth rate of 9.4 nm hr^{-1} over 8 hours, consistent with NPF observations from urban environments (Kuang et al. 2009). TDCIMS-measured species were normalized by collected particulate mass and classified into subgroups of oxygen-, nitrogen- and sulfur-containing organic compounds (i.e., CHO, CHON, CHOS, CHONS), and organic or inorganic sulfate (SOx). CHOS, CHONS, and SOx showed statistically significant higher concentrations during the NPF event with P values of 0.018, 0.014, and 0.0011,

Accepted for publication in *Bulletin of the American Meteorological Society.* DOI 10.1175/BAMS-D-23-0331.1.

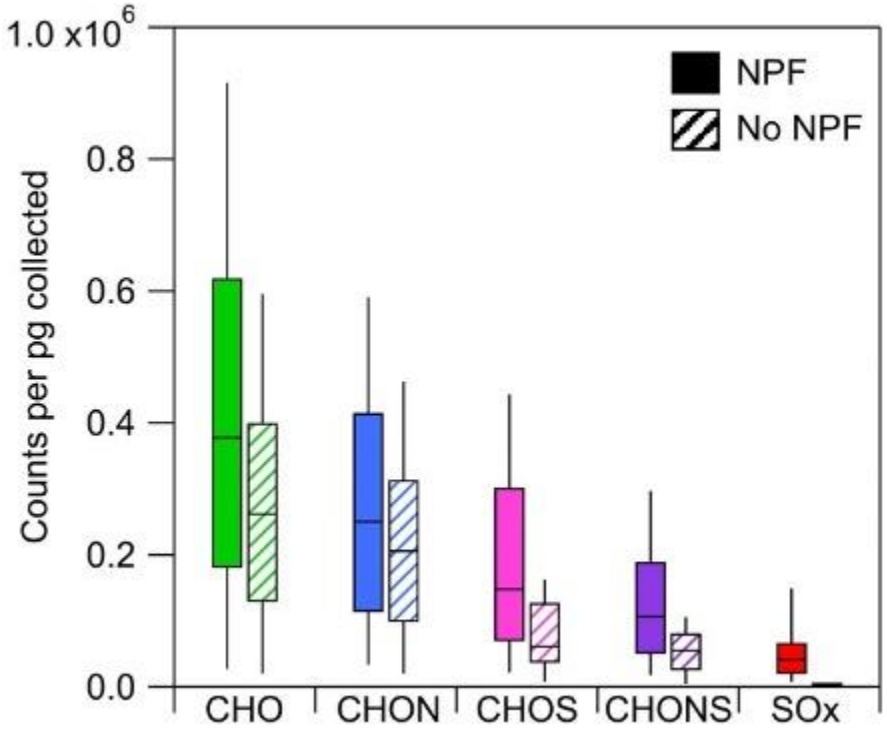

Fig. 4. TDCIMS-measured sample mass-normalized composition of 30 nm particles during an NPF event on 10 July 2022 compared to a non-event day on 21 July 2022. Box-whisker plots show the average value (horizontal line), interquartile range (box), and minimum and maximum values (whiskers).

respectively, indicating the significant role played by particulate sulfate formation in NPF and growth during this period. Sulfate was also found to be a significant fraction of the coating (26%) for particles containing black carbon (Farley et al. 2024), which were characterized by relatively thin coatings and a strong diurnal variability in number fraction (Kasparoglu et al. 2024a). Differences in both CHO and CHON were found not to be statistically significant between periods ($P > 0.05$); however, these classes dominated the composition by mass. Atomic ratios of oxygen to carbon in the CHO and CHON classes were higher for the NPF event compared to the non-event, indicating that newly formed particles had more oxidized, aged organics compared to the non-event particles. The important roles of both sulfate and organic materials in NPF and growth are further supported by additional TRACER studies that focused on the hygroscopicity of the growing nucleation mode (Kasparoglu et al. 2024b).

b. Influences of Local Meteorology on Air Pollution

Accepted for publication in *Bulletin of the American Meteorological Society.* DOI 10.1175/BAMS-D-23-0331.1.

To predict and mitigate poor air quality events in an urban coastal region an improved understanding of the links between meteorological factors such as temperature, humidity, winds, solar radiation and urban heat islands, and pollutant variability is necessary. TAQ was aptly timed with September generally being one of the more ozone polluted times of the year, resulting in many exceedance days sampled between 2021 and 2022. One of the more studied cases occurred on 9 September 2021, with results discussed observationally (Griggs et al., 2024; Sullivan et al., 2023) and with air quality modeling (Li et al., 2023; Liu et al., 2023; Soleimanian et al., 2023). On this day, the G-V mapped the Houston region three times spanning the morning, midday, and afternoon, with the objective of simulated expected measurements in preparation for the now-ongoing geostationary satellite-based air quality observations from TEMPO (https://tempo.si.edu/). Figure 5a,b shows urban emissions of NO_2 (an ozone precursor) in the morning with peaks near downtown Houston and the Houston Ship Channel. Pandora spectrometer profiles demonstrate that most of this NO_2 was confined to a few hundred meters above the

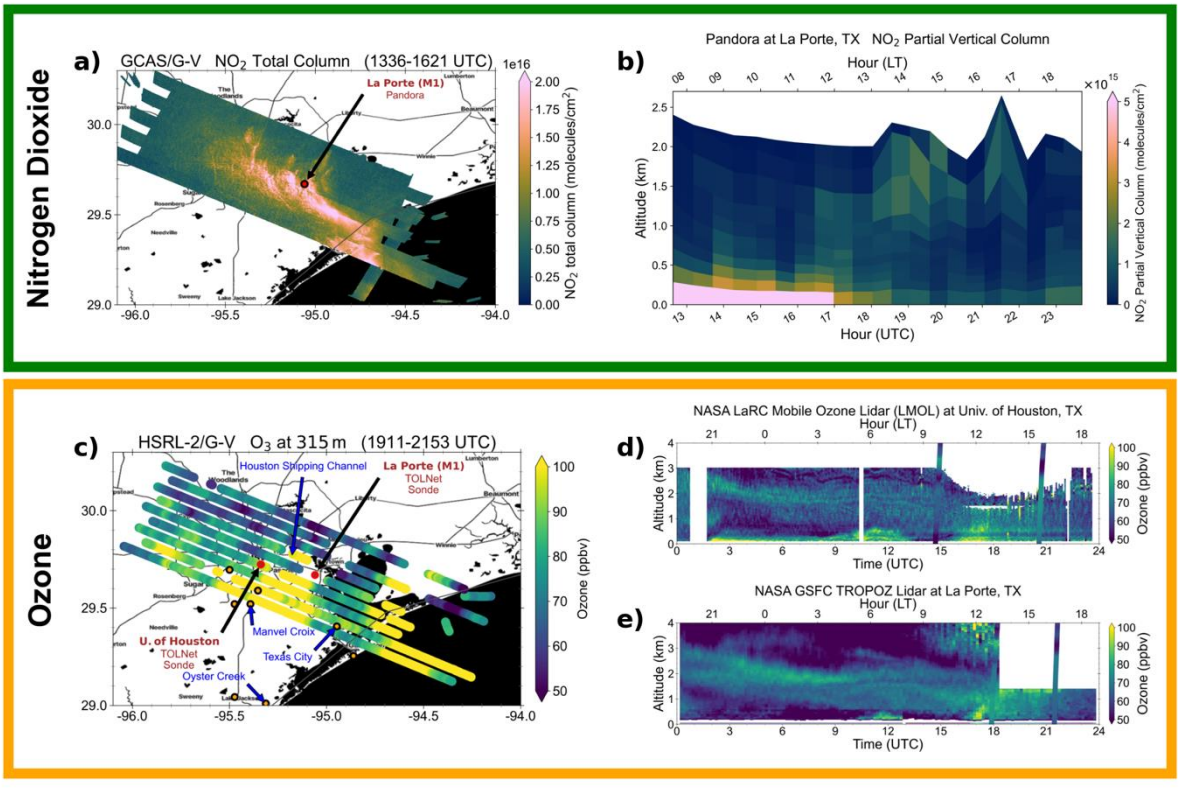

Fig. 5. Select airborne and ground-based remote sensing observations from 9 September 2021 during the TRACER-AQ campaign in Houston, TX. *Top panel:* (a) Total NO_2 column measurements during first raster (1336-1621 UTC; 0836-1121 LT) and (b) Pandora ground-based remote sensing Pandora NO_2 partial vertical column observations throughout the day. *Bottom panel:* (c) Aircraft-based O_3 mixing ratio at 315 m AMSL during the third raster (1911-2153 UTC; 1411-1653 LT). The locations of monitoring sites that

Accepted for publication in *Bulletin of the American Meteorological Society.* DOI 10.1175/BAMS-D-23-0331.1.

exceeded the 8-hr ozone standard are shown by the black-outlined orange dots. (d) TOLNet O_3 mixing ratio with coincident balloon-borne in situ O_3 profiles overlaid.

surface. Clear skies and favorable photochemical conditions fostered rapid O_3 production and led to ozone levels above the 8-hr ozone standard of 70 ppbv at monitoring sites southwest of Houston (Fig. 5c), such as the TCEQ Manvel Croix Park (79 ppbv) monitor. With winds transporting the urban emissions out over water that later were transported back to land with the SB, some of the highest maximum daily 8-hr surface ozone levels were observed at TCEQ monitors along the coast, e.g., the Texas City (75 ppbv) and Oyster Creek (81 ppbv) monitors. This synergistic suite of profiling observations provides novel and unseen perspectives in the spatial and temporal distribution of the key photochemical species and atmospheric structure, particularly with a focus on the daytime evolution of observations.

c. Detailed Observations of the Sea Breeze Circulation

The frequency of occurrence, timing, inland propagation speed and extent, and PBL interactions of the SB and Gaveston bay breeze (BB) are important factors for the cloud, aerosol, meteorological, and air quality characteristics in SE Texas (e.g., Caiendo et al, 2019; Wang et al. 2024; Rapp et al. 2024; Sharma et al. 2024; Deng et al. 2025). Using data collected from three boundary-layer profiling systems (Wagner et al. 2019) deployed along a north-south transect from the UHCC to Aldine, Klein et al. (2023) found that 41% of days during the TRACER+ IOP exhibited a SB, with a total of 50 SB cases observed by at least one of the instrument platforms. Of the observed cases, 25% did not propagate far enough inland to reach the Aldine site and/or were too diffuse to have noticeable effects on the kinematics and thermodynamics within the PBL. The average time for the SB to propagate approximately 62 km from the UHCC to Aldine was 4.5 hours but ranged from 0.75 to 6.25 hours.

An example of the observations from 9 July 2022 shows a SB passing over UHCC at 1900 UTC and reaching Aldine at 2330 UTC (Figure 6). Aldine also experienced a BB earlier in the afternoon at 2100 UTC, evident via an increase in wind speeds from 1-3 m s^{-1} to 5-7 m s^{-1}. The SB effects on the PBL are evident at the UHCC, with an increase in wind speed magnitude like that observed from the BB at Aldine. PBL moistening occurred during the SB passage, with an increase in the water vapor mixing ratio from 13-15 g kg^{-1} to > 22 g kg^{-1} from the surface to 750 m AGL. Vertical velocity observations indicate strong ascent (> 2 m s^{-1}) in the 30 minutes prior to SB passage, with decreased vertical velocity magnitudes thereafter.

Accepted for publication in *Bulletin of the American Meteorological Society.* DOI 10.1175/BAMS-D-23-0331.1.

There are also noticeable decreases in the PBL height after the SB front passage, consistent with numerous observed SB events during the TRACER+ IOP (Storm et al. 2025; Fig. 6c).

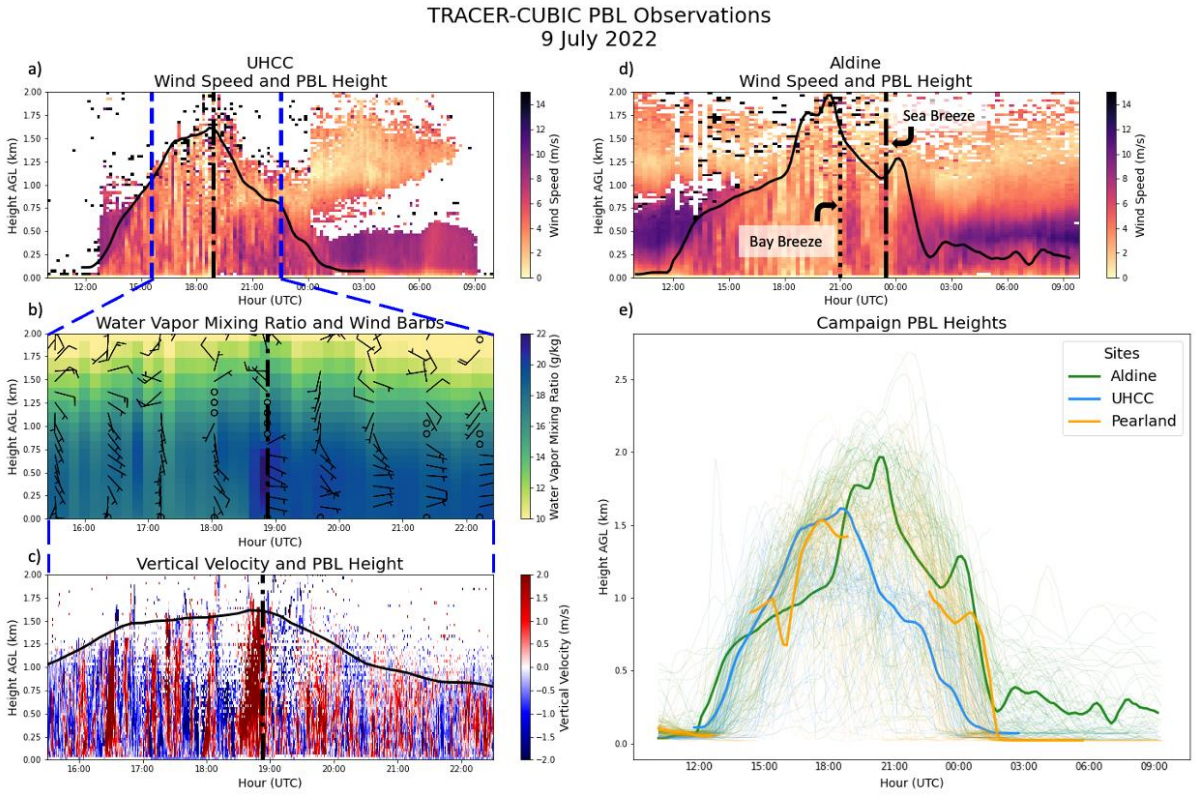

Fig. 6. 9 July 2022 PBL observations for: a) UHCC wind speed (m s^{-1}) and PBL height (black line) from 1000 - 1000 UTC, dash-dot line = SB, blue dashed line = SB analysis window, b) UHCC retrieved water vapor mixing ratio (g kg^{-1}) and wind barbs (circle = calm, half-barb = 5 m s^{-1}, full barb = 10 m s^{-1}) from 1530 - 2230 UTC, c) UHCC Doppler lidar vertical velocity (m s^{-1}) and PBL height from 1530 - 2230 UTC, d) Aldine wind speed (m s^{-1}) and PBL height from 1000 - 1000 UTC, dotted line = bay breeze, and e) estimated PBL heights (Aldine = green, UHCC = blue, Pearland= orange; thin lines = daily heights for entire campaign, bold lines = 9 July 2022 heights).

Figure 7 provides an example of sUAS-based observations of a SB event observed at the Brazoria site (29° 8' 34.8" N, 95° 19' 19.2" W) on 23 June 2022. In this figure, instantaneous profile data from the University of Oklahoma rotary wing CopterSonde sUAS are shown as colored contours, while data from the University of Colorado Robust Autonomous Airborne Vehicle - Endurant and Nimble (RAAVEN) fixed-wing sUAS (de Boer et al. 2022; 2023) are included to represent average values from its level-leg transects. Additional information on the platforms and their sampling during TRACER can be found in Lappin et al. (2024). On this day, the PBL started to develop under light (~2-3 m s^{-1}) northwesterly winds. Through the morning, winds were light and variable, until the SB front passed through the sampling location around 1830 UTC. At that time, wind speeds increased significantly (~5-7 m s^{-1}) and shifted to southeasterly. Along with this wind shift, there was a notable pause in PBL development, with

Accepted for publication in *Bulletin of the American Meteorological Society*. DOI 10.1175/BAMS-D-23-0331.1.

temperatures decreasing and RH increasing following the SB passage. Comparing the turbulence characteristics pre-SB (1730 UTC) to post-SB (2000 UTC), there is a decrease in vertical velocity variance and TKE after the SB (Fig. 7). After the SB front passage, aerosol particle concentrations decreased notably, despite greater wind speeds during this time.

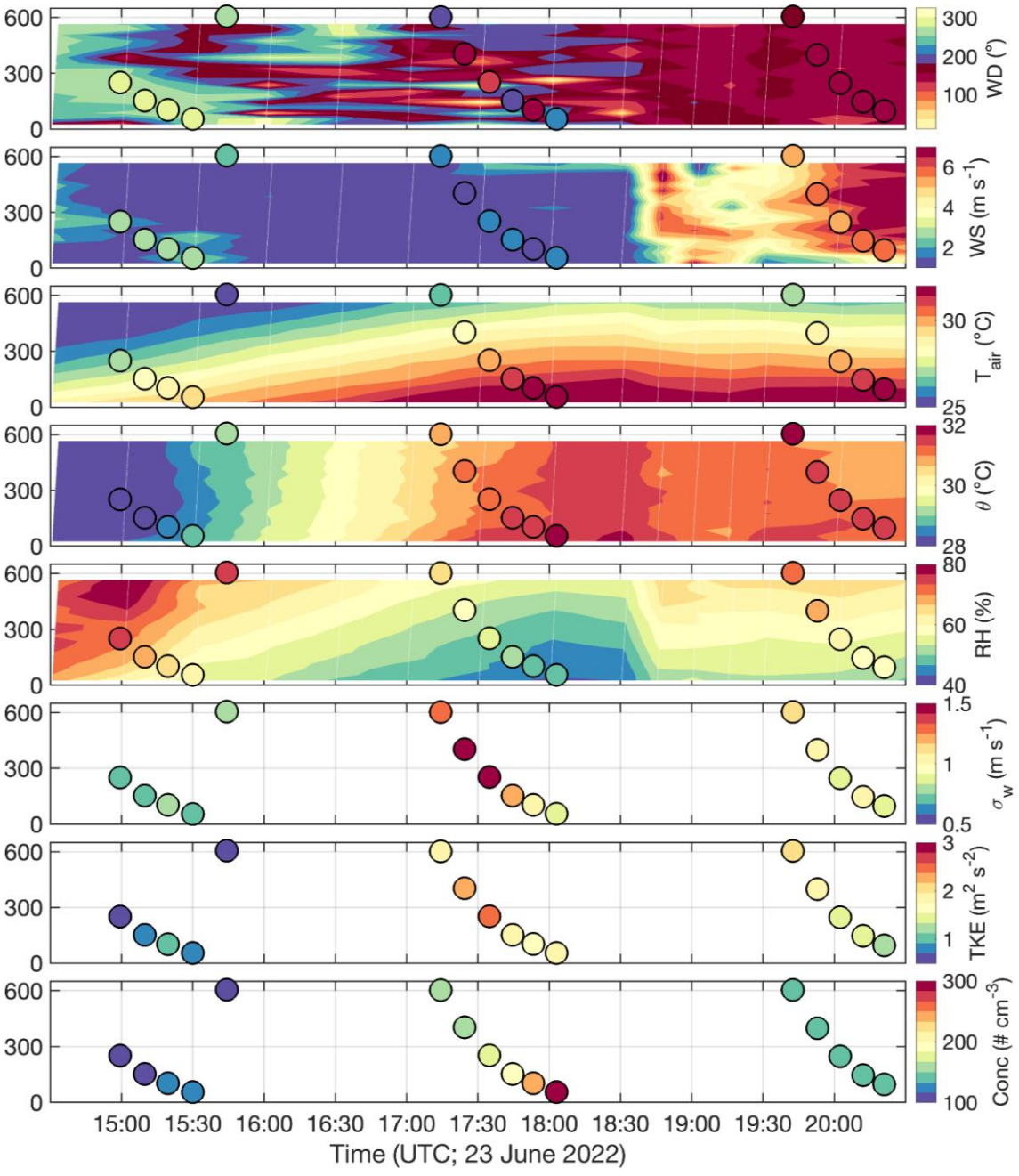

Fig. 7. Time-height cross sections of (top to bottom) wind direction, wind speed, air temperature, air potential temperature, relative humidity, vertical velocity variance, turbulent kinetic energy, and accumulation mode (150-2500 nm) aerosol particle concentration, as observed on 23 June 2022 near the Brazoria National Wildlife Refuge. Background shading is from data collected by the CopterSonde2, while the dots represent average values collected during constant altitude holds of around 9 minutes each by the RAAVEN. Vertical velocity variance, TKE, and accumulation mode aerosol concentration were only observed by the RAAVEN.

Accepted for publication in *Bulletin of the American Meteorological Society*. DOI 10.1175/BAMS-D-23-0331.1.

d. Retrieved Supersaturation in Convective Updrafts

Airborne data acquired during ESCAPE are used to test the hypothesis that aerosols can strengthen convective updrafts due to increased latent heating from nucleation of CCN above cloud base, namely through the condensational invigoration mechanism (Fan et al. 2007, 2018; Grabowski and Jarecka 2015; Grabowski and Morrison 2016; Igel and van den Heever 2021). For this mechanism to be plausible, the presence of large supersaturations (~10%) are required in pristine conditions (Romps et al. 2023). Patil et al. (in prep.) show that supersaturations greater than 5% occurred only twice, all in conditions of updrafts > 4 m s^{-1}, whereas saturations greater than 2% were more common, occurring 50 times.

Because the supersaturation inside clouds cannot be directly measured, it is approximated following the method outlined by Romps et al. (2023). This assumes quasi-steady water vapor diffusion onto observed cloud droplets considering the observed vertical velocity and is thus called the quasi-steady state supersaturation (S_{QSS}). Observations close to cloud base and cloud edge are neglected in the following analysis because of limitations of the quasi-steady state assumption in those regions. Figure 8 shows an example of a retrieved median 1-Hz S_{QSS} of 1.9% with peak up to 11% in a cloud core with updraft speeds up to 20.9 m s^{-1} sampled by the NRC Convair-580 on 9 June 2022 between 20:53:21 and 20:53:35 UTC. With aerosol concentrations of ~1000 cm^{-3} at 300 m below cloud base and back trajectory analysis (not shown) indicating an air source within the Gulf, these measurements were obtained in a relatively clean moisture-rich maritime air mass that can contribute to high supersaturations when cooled by substantial lift. At the time of the peak S_{QSS} (20:53:33 UTC), the Cloud Droplet Probe (CDP) measured a very low cloud droplet concentration of 18 cm^{-3}, a low LWC of 0.08 g m^{-3} estimated from the CDP size distributions. This is consistent with the low LWC measured by the Nevzorov probe (0.15 g m^{-3}). Additionally, large rainwater content (1.4 g m^{-3}) was estimated from the size distributions measured by the two-dimensional stereo probe (2DS); the concentration at this time was 1.4 cm^{-3}. Although the dry-bulb temperature in the updraft core was about -13°C, the 2DS images revealed very few ice particles with spherical supercooled water droplets dominating. High supersaturation zones appeared above the high reflectivity core (> 50 dBz), within reflectivity values near 40 dBz; Doppler velocities are consistent with the strong updraft. The coincidence of strong vertical velocities and enhanced supercooled water aligns with the thermal-microphysics analysis of simulated isolated deep

Accepted for publication in *Bulletin of the American Meteorological Society.* DOI 10.1175/BAMS-D-23-0331.1.

convection over Houston (Hernandez-Deckers et al. 2022). A more complete analysis of the cloud and radar conditions present at the time of high supersaturations through analysis of all sampled warm updraft core segments is provided by Patil et al., (in prep.).

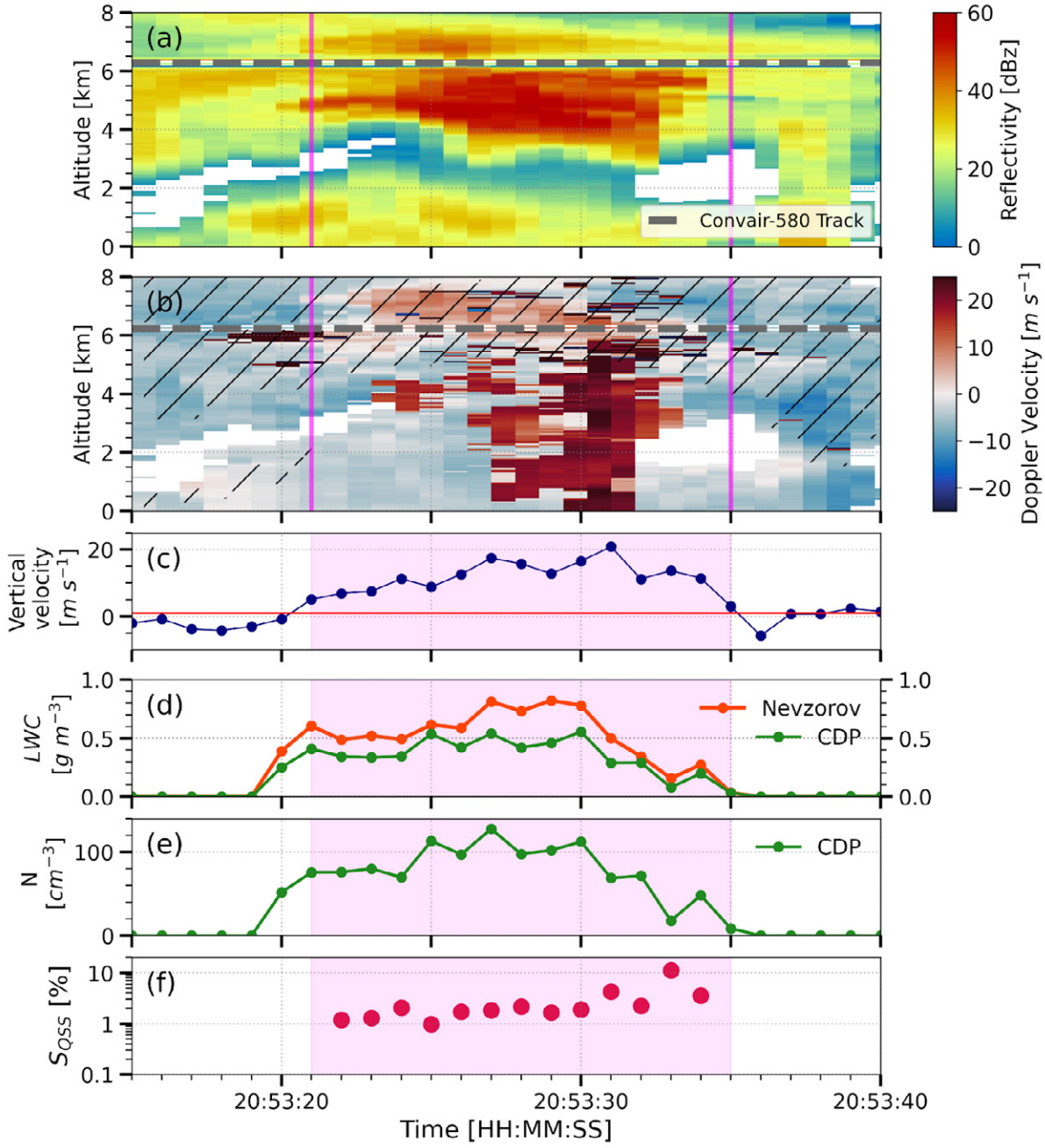

Fig. 8. Example of extreme quasi-steady state supersaturation found in a strong warm updraft core sampled in CRF06 (9 June 2022) from ESCAPE field campaign. Panel (a) shows the reflectivity of sampled thunderstorm from airborne X-band radar, panel (b) shows the doppler velocity where red color indicates upward and blue is downward velocities. Stippling on panel (b) shows the de-aliased doppler velocity using dual frequency technique and is limited due to attenuation of the W-band frequency. The dashed gray line in panels (a) and (b) is the NRC Convair-580 flight path. The time series in panel (c) is of in-situ measured vertical velocities using Aircraft Integrated Meteorological Measurement Systems (AIMMS-20) probe. Vertical velocity observations above solid horizontal red line (+1 m s^{-1}) are updrafts. Panel (d) shows Liquid

Accepted for publication in *Bulletin of the American Meteorological Society.* DOI 10.1175/BAMS-D-23-0331.1.

water Content (LWC) using Nevzorov probe (red color) and CDP (green color). Panel (e) shows number concentration of cloud droplets (D < 50 μm) (N) from CDP and panel (f) shows quasi-steady state supersaturations (S_{QSS}) estimated using Romps et al. (2023) method. The vertical magenta lines in panels (a), (b) and the area highlighted with magenta in panels (c) – (f) shows the duration of the objectively identified intense updraft core segment using 1 Hz in-situ observations.

e. Characterizing the Convective Updraft Lifecycle

One of the most significant challenges of the observational study of convective cloud lifecycle is achieving the high spatial and temporal resolution with remote sensing to capture the rapid evolution of the dynamical and microphysical properties of the convective core. The vertical cross-section scans collected by the CHIVO and CSAPR2 radar through evolving convection offer an unprecedented opportunity to examine the evolution of convective updrafts (e.g., Dolan et al. 2023; Lamer et al. 2023). Kollias et al. (2025) use the radial Doppler velocity measurements collected by the scanning radars to estimate vertical air motion using high elevation angle RHI from a single radar. The technique accounts for the hydrometeor sedimentation velocity using the hydrometeor ID derived from the radar polarimetry and reflectivity measurements and for the horizontal wind using the convective core lateral edges. Detailed error analysis indicates that the error in the estimation of the convective motion is below 5 m s^{-1} at an elevation angle above 30 degrees. Figure 9 presents the retrieved vertical air motions and observed radar reflectivity from consecutive radar scans guided by the MAAS-framework targeting the same location within a storm. These coherent updrafts exhibit intricate, coherent "thermal-like" (e.g., Matsui et al. 2024) dynamical structures, with widths ranging from < 1 km to ~5 km. Over the 50-s observation period, the overall shape of the coherent updraft changed minimally, with an intense vertical velocity of 20-30 m s^{-1} observed. Further analysis of nearby vertical cross-sections could also yield insights into the spatial displacement of the strongest updraft core within the storm during its life cycle. These observations thus motivate further investigation into the key drivers of convective microphysics.

f. Variability in Lightning Characteristics of Convective Storms

Changes in lightning flash rates, location and other characteristics provides important constraints for understanding convective storm intensity and evolution, cloud and precipitation microphysics, and storm morphology and hazards, The lightning observations (Logan et al. 2023) during the TRACER+ IOP are summarized by Bruning et al. (2024). On 25 days with

Accepted for publication in *Bulletin of the American Meteorological Society.* DOI 10.1175/BAMS-D-23-0331.1.

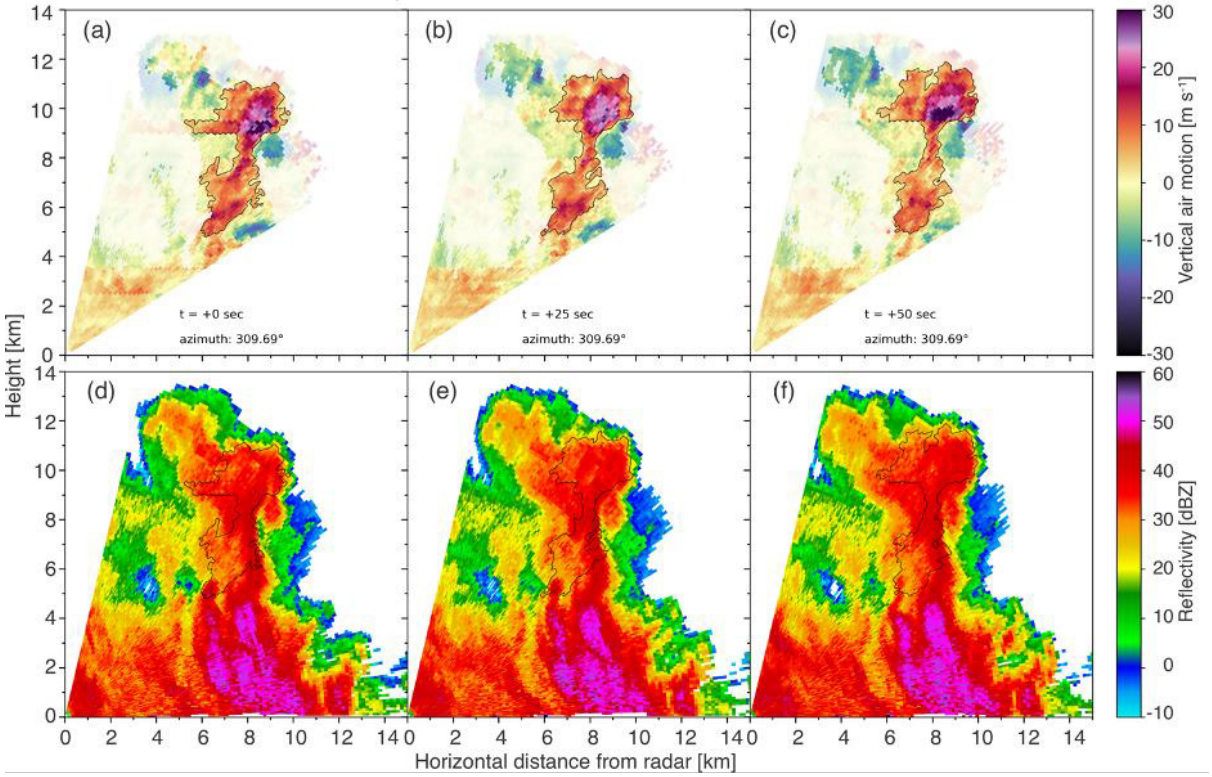

Fig. 9. Vertical cross sections of (a-c) vertical air motion retrieved following Kollias et al. (2025) above 30 degree elevation and (d-f) radar reflectivity observed in consecutive CHIVO RHI scans toward an azimuth angle of 309.7° on 16 September 2022 from 07:58:05 UTC every 25 seconds. The black outline in each panel encompasses the regions with updrafts greater than or equal to 3 m s^{-1}. For emphasis, regions of reflectivity < 25 dBZ are faded in panels a-c.

lightning that were also well-forecast by real-time NU-WRF (Peters-Lidard et al. 2015) simulations, 7488 storms within 90 km of the KHGX NEXRAD were identified and tracked (using *tobac)* through their lifecycle. In each tracked storm, the time series of lightning flash rates and the strength of mixed-phase columns of enhanced polarimetric variables (differential reflectivity [Z_{DR}] and specific differential phase [K_{DP}]) were also quantified. These measures serve as a proxy for updraft depth and the strength (Kumjian et al. 2014) of activation of mixed-phase processes; the absence of any of these signals indicates a storm where warm rain formation processes dominate (van Lier-Walqui et al. 2016). As expected, strong covariance was found among the occurrence of Z_{DR} and K_{DP} columns, and lightning was observed to generally require the presence of a Z_{DR} column and often a K_{DP} column. Lightning did not covary as strongly with polarimetry as the polarimetric measures did among themselves, indicating that it adds independent information about precipitation process dynamics.

The variability in the thermodynamic and aerosol properties of air masses is illustrated in the fraction of tracks observed to have deep polarimetric columns and lightning. These fractions varied by tens of percent from day to day, and at times half the population with Z_{DR}

Accepted for publication in *Bulletin of the American Meteorological Society.* DOI 10.1175/BAMS-D-23-0331.1.

and K_{DP} columns had lightning and half did not, further illustrating the additional signals of mixed-phase precipitation process intensity signaled by lightning. There was low-to-nonexistent covariance of the track fractions with the CCN concentrations and entraining CAPE (ECAPE; Peters et al. 2023) measured at the AMF1 site.

Figure 10 shows a further analysis of the same cell-tracking data but segregated into the locations of the tracks relative to the SB boundary, i.e., on either side of or crossing the boundary. A more refined CCN concentration and ECAPE value was assigned to each track by interpolating soundings from the AMF1 and mobile platforms (Rapp et al. 2024) in space and time. Clear differences in lightning track fractions were observed for the cells crossing

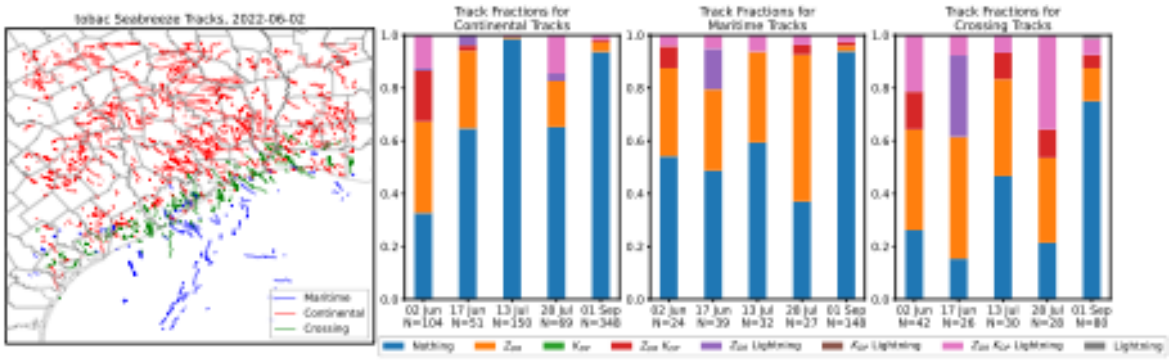

Fig. 10. Lightning and polarimetry in tracked storms, divided by location relative to the sea breeze front. (a) Track locations and air mass classifications on 2 June 2022, (b, c, d) polarimetric classification and lightning presence (as indicated in the legend) on five selected days during the TRACER campaign by air mass.

the SB boundary, with more subtle differences between the continental and maritime populations. On three of the five days presented in Figure 10, a much larger lightning fraction implies that a mix of dynamical forcing along the SB boundary plus local blending of airmass properties was responsible for greater vigor of mixed-phase drafts. For the two case days studied to date across a few thousand tracks, low and high flash rates were observed across all CCN and ECAPE values, indicative of a need to continue to assess other cases in large statistical numbers while also accounting for the environmental heterogeneity.

g. Urban Influences on Surface Fluxes

Surface energy fluxes, particularly the balance between sensible and latent heat, are an important driver of variability of the boundary layer heat budget. These fluxes are strongly modulated by the surface type with gradients between rural and urban areas driving the UHI effect. Figure 11 shows the difference in hourly averaged surface energy fluxes for the IOP period at four representative measurement sites: urban (UHMT), rural (LIB), coastal (UHCC), and bay (AMF1). The coastal site has the highest peak sensible heat flux (SHF) of about 225

Accepted for publication in *Bulletin of the American Meteorological Society*. DOI 10.1175/BAMS-D-23-0331.1.

Wm^{-2}, followed by the urban, rural, and bay sites. The SHF at the urban site always remains positive, even during the nighttime, while at all other sites, the average SHF is negative between 0000-1000 UTC. The lower SHF observed at the urban site is typical as most of the incoming solar radiation is absorbed within the built environment as storage heat flux, which is then emitted as sensible heat following peak solar insolation. High latent heat fluxes (LHF) are observed at the coastal and bay sites (peak values > 200 W m^{-2}), whereas LHF values are much lower at the rural site (peak value ~145 W m^{-2}). The LHF signal at the urban site is irregular as it was mostly forced by intermittent precipitation events. In the rural location, where transpiration from vegetation is normally a significant contributor to LHF, lower values are found due to a dry summer season with low soil moisture. Overall, the figures high spatial

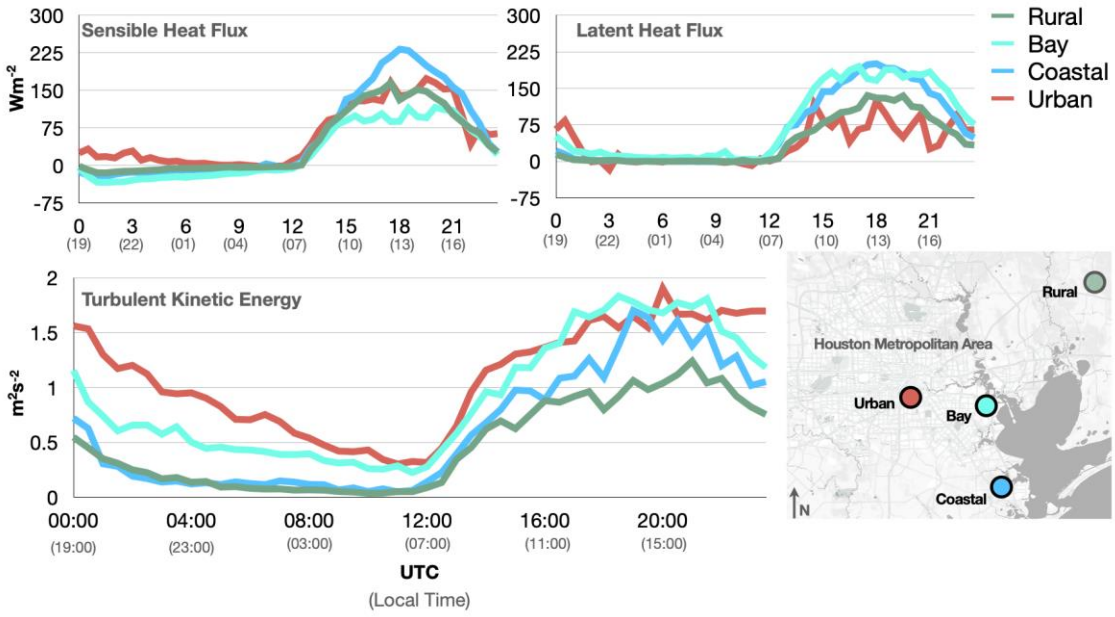

Fig. 11. Diurnal cycle of hourly averaged surface energy fluxes (SHF, left; LHF right) at all four sites for the summer period. Averaged hourly variation in TKE during the summer months (bottom left). Map of the relative location of the four surface flux sites deployed for CUBE.

gradients in surface energy fluxes that can influence convective cloud processes are found and the average TKE values at the four sites show distinct diurnal variability. Due to increased aerodynamic roughness, the urban site experiences higher TKE compared to all other sites, followed by the bay site, which is surrounded by residential buildings. The rural site experiences relatively low TKE values. The coastal site, which is consistently influenced by thermally driven SB winds, has high TKE values during the daytime.

h. Other TRACER+ early research

Accepted for publication in *Bulletin of the American Meteorological Society*. DOI 10.1175/BAMS-D-23-0331.1.

In addition to the research highlights presented above, TRACER+ research activities are also being undertaken to address fundamental questions on the lifecycle of cloud, aerosols and pollutants in the coastal-urban environment. Specifically, a sampling of these research activities includes: development of methods for the correction of filter-based aerosol light absorption biases (Kumar et al. 2024), the study of vertical profiles of CCN and INP using combined remote sensing and surface-based in situ measurements (Chen et al. 2025), the influence of the coastal environment on ozone formation and regional variability, neighborhood-level inequities of air pollution (Dressel et al. 2024), SB impacts on boundary layer aerosol populations (Subba et al. 2025), convective mixed-phase processes and their interactions with the environment, variability of convective cells as a function of cloud lifecycle (e.g., Mages et al. 2024, Tuftedal et al. 2024), the influence of mesoscale initiation on the subsequent evolution of convective cells (e.g., Hahn et al. 2025), influence of urban features on cloud development, causal analysis of aerosol-convection interactions (Wang et al. 2025), and environmental and cloud property influences on precipitation formation and microphysics.

5. Future TRACER+ research – The TRACER MIP

A major initiative of the TRACER campaign is to follow the ACPC MIP with a new TRACER-MIP (Fan et al. 2024) that leverages new and comprehensive measurements to: (i) quantify the inter-model spread in representation of aerosol-convection interactions, identify model deficiencies, and measure model performance; and (ii) examine the factors and processes leading to model biases and large model spread. Two "golden" convective case study events were identified with varying dynamic, thermodynamic, and aerosol conditions for the TRACER-MIP simulations. The 17 June and 7 August 2022 events (Figure 12) were enhanced operations days (Figure S4) and chosen based on the presence of a distinct SB circulation, observed scattered convective cells, and the availability of SMPS data, CSAPR2 cell tracking, large differences in lightning occurrence (Bruning et al. 2024) and frequent soundings. The 17 June case had widespread convection, featuring afternoon SB-induced thunderstorms in an environment with high aerosol concentrations (~4000 cm^{-3}; > 10 nm diameter). The 7 August case had a morning SB circulation and thunderstorms in the early afternoon with relatively cleaner aerosol conditions (~1700 cm^{-3}; > 10 nm diameter). With comprehensive observations, this MIP can uniquely help evaluate model deficiencies and shine a light on further improving

Accepted for publication in *Bulletin of the American Meteorological Society.* DOI 10.1175/BAMS-D-23-0331.1.

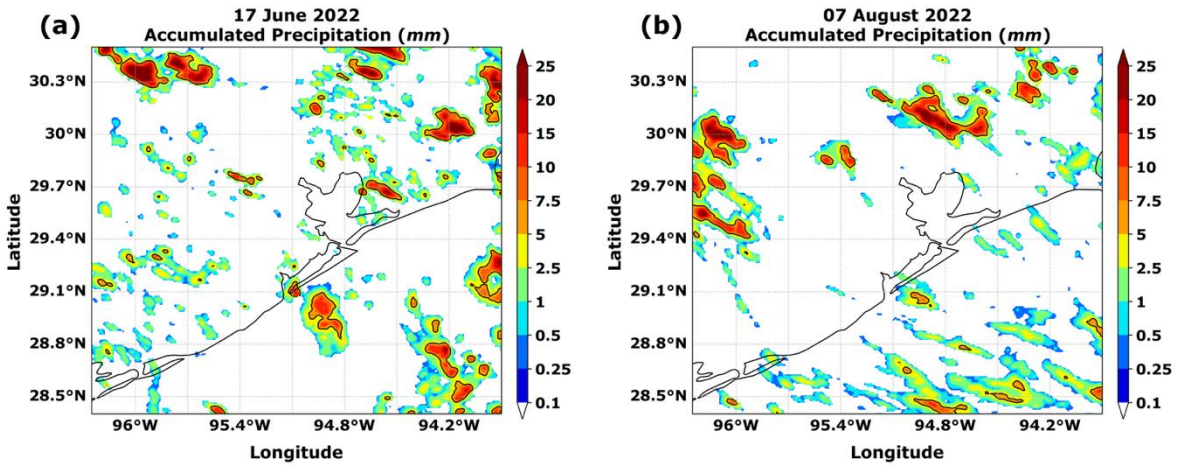

Fig. 12. 18-hour accumulated precipitation starting 0700 LT on (a) 17 June 2022 and (b) 07 August 2002 from the Multi-Radar/Multi-Sensor System (MRMS) 1-km gridded dataset.

model predictable capabilities. Efforts are underway to assemble comprehensive observational datasets to support the TRACER-MIP activities (e.g., Lamer et al. 2024).

Simulations of the TRACER-MIP cases have been completed with the Regional Atmospheric Modeling System (RAMS), and the *tobac* feature tracking algorithm has been applied to the high-frequency output to identify and track mid-level updrafts (i.e., cells) with velocity greater than 3, 5, and 10 m s^{-1}. The fields related to the tracked cells (with lifetimes > 25 min) were then averaged within individual cell cores over all identified cells to generate cell core composites distributed across altitude and normalized time. Figure 13 displays normalized- time-height composites of (a) updraft strength (m s^{-1}) from the lowest aerosol

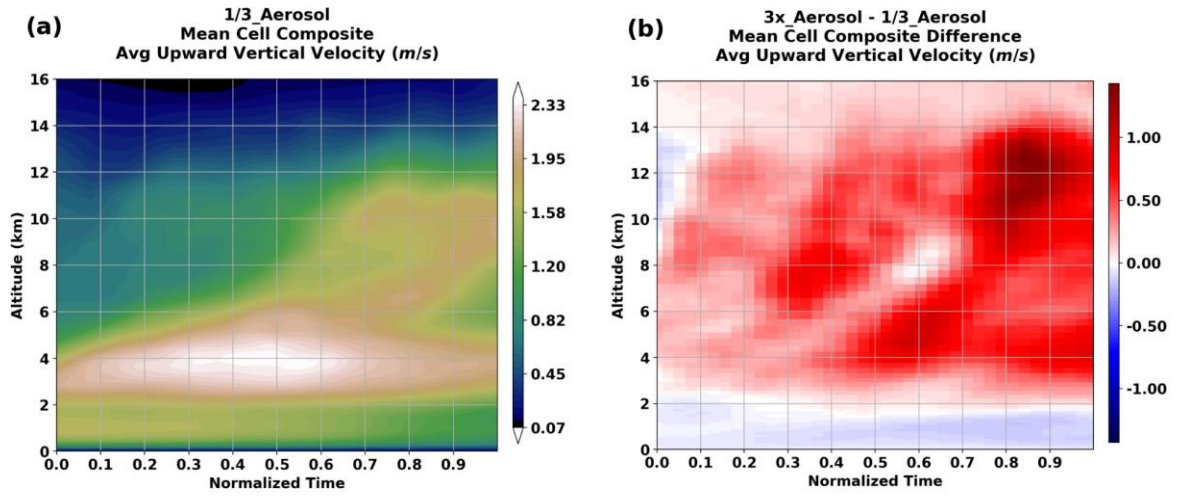

Fig. 13. Time-height plots of cell composites of: (a) the mean updraft speed (m s^{-1}) from the lowest aerosol concentration simulation, and (b) the difference field taken as Highest - Lowest aerosol simulations. Time is on a normalized cell lifetime scale where 0.0 is the first and 1.0 is the last identified cell time.

Accepted for publication in *Bulletin of the American Meteorological Society.* DOI 10.1175/BAMS-D-23-0331.1.

simulation of the 17 June event and the (b) related difference field computed as results from the highest minus lowest aerosol simulations. The development, growth, and decay of the updrafts over cell lifetime are seen and the updrafts transition to greater depth toward the latter period (Fig. 13a). Increasing aerosol concentrations leads to increased updraft strength above 2 km AGL and decreased updraft strength below 2 km (Fig. 13b). The aerosol-induced changes to updraft strength may result from a combination of changes in microphysics, dynamics, and environment (e.g., Marinescu et al. 2021). Further examination of MIP model simulations will assist in determining the cause of changes in simulated convective characteristics in these events towards establishing the relative importance of the factors (e.g., dynamics, buoyancy, aerosol) that control the characteristics of convective drafts in nature.

Acknowledgments.

Overall support for the TRACER+ field campaigns was from the DOE ARM facility and ASR program (TRACER), the NSF Physical and Dynamic Meteorology Program (ESCAPE and CUBE), NASA's Tropospheric Composition and Health and Air Quality Sciences programs (TAQ) and the TCEQ (TAQ and TAQ2). We acknowledge the important contributions of the ARM AMF1 site operations staff members, the University of Houston, the NASA Gulfstream-V flight and support crews, the NRC Convair flight and support crews, the SPEC Learjet flight and support crews, Tim Berkoff (NASA LaRC) and Barry Lefer (NASA headquarters). We acknowledge specific DOE contracts DE-SC0012704, DE-SC0021047, DE-SC0021074, DE-SC0021160, DE-SC0021242, DE-SC0021247, DE-SC0021381, DE-SC0022140, DE-SC0025214, NSF contracts AGS-2019649, AGS-2019932, AGS-2019939, AGS-2019947, AGS-2019968, AGS-2020000, Geo 1802226, and TCEQ contracts 582-21-11425-009, 582-21-22317-015, 582-22-31913-019, 582-22-31913-020, 582-22-31544-019. TAMU undergraduate participants were also supported by a Texas A&M University College of Arts and Sciences (formerly Geosciences) High-Impact Learning Experience grant. The content, findings, opinions, and conclusions are the work of the authors and do not necessarily represent the findings, opinions, and conclusions of the TCEQ.

Accepted for publication in *Bulletin of the American Meteorological Society.* DOI 10.1175/BAMS-D-23-0331.1.

Data Availability Statement.

Data collected during the TRACER+ field campaigns is available via the associated agency data repositories. Data collected as part of the TRACER campaign is available through ARM data discovery (https://www.arm.gov/data) after registering for a free account. All ESCAPE data are cataloged at the NCAR EOL ESCAPE data archive: https://data.eol.ucar.edu/project/ESCAPE. Data from TRACER-AQ are available on the NASA TRACER-AQ data archive: https://www-air.larc.nasa.gov/missions/trsacer-aq/.

REFERENCES

Bean, J., C. Faxon, Y. Leong, H. Wallace, B. Cevik, S. Ortiz, M. Canagaratna, S. Usenko, R. Sheesley, R. Griffin, and L. Hildebrandt Ruiz. 2016: Composition and sources of particulate matter measured near Houston, TX: Anthropogenic–biogenic interactions. *Atmosphere* **7(5)**:73. https://doi.org/10.3390/atmos7050073

Brock, C.A., M. Trainer, T.B. Ryerson, J.A. Neuman, D.D. Parrish, J.S. Holloway, D.K. Nicks, G.J. Frost, G. Hubler, F. C. Fehsenfeld, J. C. Wilson, J. M. Reeves, B. G. Laflwur, H. Hilbert, E. L. Atlas, S. G. Donnelly, S. M. Schauffler, V. R. Stroud, and C. Weidinmyer, 2003: Particle growth in urban and industrial plumes in Texas. *J. Geophys. Res. Atmos.* **108** (D3):12. https://doi.org/10.1029/2002jd002746.

Bruning, E. C., K. N. Brunner, M. van Lier-Walqui, T. Logan and T. Matsui, 2025: Lightning and radar measures of mixed-phase updraft variability in tracked storms during the TRACER field campaign in Houston, Texas. *Mon. Wea. Rev.*, **152**(12), 2753-2769. https://doi.org/10.1175/MWR-D-24-0060.1.

Burton, S. P., R. A. Ferrare, C. A. Hostetler, J. W. Hair, R. R. Rogers, M. D. Obland, C. F. Butler, A. L. Cook, D. B. Harper, and K. D. Froyd, 2012: Aerosol classification using airborne High Spectral Resolution Lidar measurements – methodology and examples. *Atmos. Meas. Tech.*, **5(1)**, 73–98. https://doi.org/10.5194/amt-5-73-2012

Caicedo, V., B. Rappenglueck, G. Cuchiara, J. Flynn, R. Ferrare, A. J. Scarino, T. Berkoff, C. Senff, A. Langford, and B. Lefer, 2019: Bay Breeze and Sea Breeze Circulation Impacts on the Planetary Boundary Layer and Air Quality from an Observed and Modeled

Accepted for publication in *Bulletin of the American Meteorological Society.* DOI 10.1175/BAMS-D-23-0331.1.

DISCOVER-AQ Texas Case Study. *J. Geophys. Res. – Atmos.*, **124**(13): 7359–7378, https://doi.org/10.1029/2019jd030523

Chen, B., S. A. Thompson, B. H. Matthews, M. Sharma, R. Li, C. J. Nowotarski, A. D. Rapp, and S. D. Brooks, 2025: A new technique to retrieve aerosol, CCN, and INP vertical profiles using the Micropulse lidar and ground-based aerosol measurements during the TRACER campaign. EGUsphere [preprint], https://doi.org/10.5194/egusphere-2024-3363.

Cheong, B. L., R. Kelley, R. D. Palmer, Y. Zhang, M. Yeary and T. -Y. Yu, 2013: PX-1000: A Solid-State Polarimetric X-Band Weather Radar and Time–Frequency Multiplexed Waveform for Blind Range Mitigation." *IEEE Transactions on Instrumentation and Measurement*, 62 (11), 3064-3072, https://doi.org/10.1109/TIM.2013.2270046.

Clothiaux, E. E., T. P. Ackerman, G. G. Mace, K. P. Moran, R. T. Marchand, M. A. Miller, and B. E. Martner, 2000: Objective determination of cloud heights and radar reflectivities using a combination of active remote sensors at the ARM CART sites, *J. Appl. Meteor.*, **39**, 645–665.

Clothiaux, E. E., M. A. Miller, R. C. Perez, D. D. Turner, K. P. Moran, B. E. Martner, T. P. Ackerman, G. G. Mace, R. T. Marchand, K. B. Widener, D. J. Rodriguez, T. Uttal, J. H. Mather, C. J. Flynn, K. L. Gaustad, and B. Ermold, 2001: The ARM Millimeter Wave Cloud Radars (MMCR2) and the Active Remote Sensing of Clouds (ARSCL) Value-Added Product (VAP), DOE Tech. Memo ARM VAP-002.1, U. S. Department of Energy, Office of Science, Office of Biological and Environmental Research, Atmospheric Radiation Measurement Facility. Germantown, MD.

Creamean, J. M., T. C. J. Hill, C. C. Hume, and T Devadoss. 2024: Ice Nucleation Spectrometer (INS) Instrument Handbook. U.S. Department of Energy, Atmospheric Radiation Measurement user facility, Richland, Washington. DOE/SC-ARM-TR-278.

de Boer, G., S. Borenstein, R. Calmer, C. Cox, M. Rhodes, C. Choate, J. Hamilton, J. Osborn, D. Lawrence, B. Argrow, and J. Intrieri, 2022: Measurements from the University of Colorado RAAVEN Uncrewed Aircraft System during ATOMIC, *Earth Syst. Sci. Data*, **14**, 19–31, https://doi.org/10.5194/essd-14-19-2022.

Accepted for publication in *Bulletin of the American Meteorological Society.* DOI 10.1175/BAMS-D-23-0331.1.

de Boer, G., P. Klein, B. Argrow, T. Thornbury, P. Chilson, R. Calmer, F. Lappin, M. Rhodes, E. Pillar-Little, B. Butterworth, A. Segales, J. Hamilton, K. Britt, J. Buchli, I. Medina, E. Asher, L. Otterstatter, M. Ritsch, B. Puxley, A. Miller, M. Spencer, C. Gomez-Falk, E. Smith, and S. Borenstein, 2023: TRACER-Uncrewed Aircraft Systems (TRACER-UAS) Field Campaign Report. U.S. Department of Energy, Atmospheric Radiation Measurement user facility, Richland, Washington. DOE/SC-ARM-23-028.

Deng, M., M. P. Jensen, S. E. Giangrande, K. L. Johnson, D. Wang, Y. Chu., K. Lamer, T. Subba and J. C. Pena, 2025: Bay Breeze Circulation with Orienteering Tape Recorder Method. *J. Geophys. Res. Atmos.,* Accepted.

Dolan B., P. Kollias, S. van den Heever, K. Rasmussen, M. Oue, E. Luke, K. Lamer, B. Treserras, Z. Haddad, G. Stephens, and V. Chandrasekar, 2023: Time Resolved Reflectivity Measurements of Convective Clouds. *Geophys. Res. Lett.*, **50**(22), e2023GL105723, https://doi.org/10.1029/2023GL105723.

Dressel, I. M. S. Zhang, M. A. G. Demetillo, S. Yu, K. Fields, L. M. Judd, C. R, Nowlan, K, Sun, A. Kotsakis, A. J. Turner, and S. E, Pusede, 2024: Neighborhood-level nitrogen dioxide inequalities contribute to surface ozone variability in Houston, Texas. *ACS ES&T Air*, **1**(9), 973-988, https://doi.org/10.1021/acsestair.4c00009.

Dzambo, A. M., E. Bruning, M. Oue, K. Brunner, D. Singewald, E. Rosky, N. Allwayin, S. Patil, Y. Qiao, Z. Xia, Y. Hu, Y. Huang, G. M. McFarquhar, P. Kollias, J. Souza, M. Miller, S. Weiss, and B. Ascher, 2024: Forecasting for ESCAPE: A multi-institution hybrid forecasting and nowcasting operation for sea-breeze convection supporting a ground-based and airborne field campaign. *Bull. Amer. Meteor. Soc*., 106(3), E456-E472. https://doi.org/10.1175/BAMS-D-23-0015.1.

Fan, J., D. Rosenfeld, Y. Zhang, S. E. Giangrande, Z. Li, L. A. T. Machado, S. T. Martin, Y. Yang, J. Wang, P. Artaxo, H. J. Barbosa, R. C. Braga, J. M. Comstock, Z. Feng, W. Gao, H. B. Gomes, F. Mei, C. Pohlker, M. L. Pohlker, U. Poschl and R. A. F. De Souza, 2018: Substantial convection and precipitation enhancements by ultrafine aerosol particles. *Science,* **359**, 411-418. https://doi.org/10.1126/science.aan8461

Fan, J., S. Saleeby, M. Jensen, S. van den Heever, P. Kollias, T. Subba, C. Kuang, B. Chen, A. D. Rapp, S. D. Brooks, M. Zawadowicz, S. Samanta and M. Oue, 2024: Tracking

Accepted for publication in *Bulletin of the American Meteorological Society.* DOI 10.1175/BAMS-D-23-0331.1.

Aerosol Convection interactions Experiment (TRACER) Model Intercomparison Project (MIP) Roadmap. https://arm-synergy.github.io/tracer-mip/Roadmap.html

Fan, J., Y. Zhang, Z. Li, J. Hu, and D. Rosenfeld, 2020: Urbanization-induced land and aerosol impacts on sea-breeze circulation and convective precipitation, *Atmos. Chem. Phys*., **20**, 14163–14182, https://doi.org/10.5194/acp-20-14163-2020.

Fan, J., R. Zhang, G. Li and W.-K. Tao, 2007: Effects of aerosol and relative humidity on cumulus clouds. *J. Geophys. Res.*, **112** (D24), https://doi/org/10.1029/2006JD008136

Farley, R. N., J. E. Lee, L.-H. Rivellini, A. K. Y. Lee, R. Dal Porto, C. D. Cappa, K. Gorkowski, A. S. M. Shawon, K. B. Benedict, A. C. Aiken, M. K. Dubey and Q. Zhang, 2024: Chemical Properties and Single Particle Mixing State of Soot Aerosol in Houston during the TRACER Campaign. *Atmos. Chem. Phys*., **24**, 3953–3971, https://doi.org/10.5194/acp-24-3953-2024.

Ferrare, R., J, Hair, C. Hostetler, T. Shingler, S. P. Burton, M. Fenn, M. Clayton, A. J. Scarino, D. Harper, S. Seaman, A. Cook, E. Crosbie, E. Winstead, L. Ziemba, L. Thornhill, C. Robinson, R. Moore, M. Vaughan, A. Sorooshian, J. Schlosser, H. Liu, B. Zhang, G. Diskin, J. DiGangi, J. Nowak, Y. Choi, P. Zuidema, S. Chellappan, 2023: Airborne HSRL-2 measurements of elevated aerosol depolarization associated with non-spherical sea salt. *Front. Remote Sens*. **4**:1143944. https://doi.org/10.3389/frsen.2023.1143944

Fridlind, A. M., M. van Lier-Walqui, S. Collis, S. E. Giangrande, R. C. Jackson, X. Li, T. Matsui, R. Orville, M. H. Picel, D. Rosenfeld, A. Ryzhkov, R. Weitz, and P. Zhang. 2019: Use of polarimetric radar measurements to constrain simulated convective cell evolution: a pilot study with Lagrangian tracking. *Atmos. Meas. Tech*., **12**(6): 2979–3000, https://doi.org/10.5194/amt-12-2979-2019

Giangrande, S. E., R. Oktem, D. Romps, and M. Jensen, 2023: Stereo Camera Deployment in Support of TRACER Field Campaign Report. U.S. Department of Energy, Atmospheric Radiation Measurement user facility, Richland, Washington. DOE/SC-ARM-23-016. https://www.arm.gov/publications/programdocs/doe-sc-arm-23-016.pdf

Accepted for publication in *Bulletin of the American Meteorological Society*. DOI 10.1175/BAMS-D-23-0331.1.

Grabowski, W. W. and D. Jarecka, 2015: Modeling Condensation in Shallow Nonprecipitating Convection. *J. Atmos. Sci*., **72**, 4661-4679. https://doi.org/10.1175/JAS-D-15-0091.1

Grabowski, W. W. and H. Morrison, 2016: Untangling Microphysical Impacts on Deep Convection Applying a Novel Modeling Methodology. Part II: Double-Moment Microphysics. *J. Atmos. Sci*., **73**, 3749-3770. https://doi.org/10.1175/JAS-D-15-0367.1.

Griggs, T., J. Flynn, Y. Wang, S. Alvarez, M. Comas, and P, Walter, 2024: Characterizing overwater high ozone events in the Houston-Galveston-Brazoria region during the 2021 GO3 and TRACER-AQ campaigns. *Bull Amer. Meteor. Soc*., **105**(4), E803-E815. https://doi.org/10.1175/BAMS-D-23-0034.s1.

Guagenti, M., S. Shrestha, M. Mehra, S. Yoon, S., M. T. S. Ramirez, J. H. Flynn, III and S. Usenko, 2025a: Temporal Profiles of Volatile Organic Compounds near the Houston Ship Channel, Texas. *Atmosphere* 2025a, **16**, 260. https://doi.org/10.3390/atmos16030260

Guagenti, M., D. Dexheimer, A. Ulinksi, P. Walter, J. H. Flynn, III, S. Usenko, 2025b: A modular approach to volatile organic compound samplers for tethered balloon and drone platforms. *Atmos. Meas. Tech.* 18 (9), 2125 – 2136. https://doi.org/10.5194/amt-18-2125-2025

Hahn, T., D. Wang, J. Chen, M. P. Jensen, 2025: Evaluating Sea Breezes and Associated Convective Cloud Evolution in the Model Gray Zone. *J. Geophys. Res*., 130(12), e2024JD042586. https://doi.org/10.1029/2024JD042586

Hanft, W. and A. L. Houston, 2018: An observational and modeling study of mesoscale air masses with high theta-e. *Mon. Wea. Rev*., **146**(8), 2503-2524. https://doi.org/10.1175/MWR-D-17-0389.1

Heikenfeld, M., P. J., Marinescu, M. Christensen, D. Watson-Parris, F. Senf, S. C. van den Heever, and P. Stier, 2019a: tobac 1.2: towards a flexible framework for tracking and analysis of clouds in diverse datasets, *Geosci. Model Dev*., **12**, 4551–4570, https://doi.org/10.5194/gmd-12-4551-2019.

Accepted for publication in *Bulletin of the American Meteorological Society*. DOI 10.1175/BAMS-D-23-0331.1.

Heikenfeld, M., B. White, L. Labbouz, and P. Stier, 2019b: Aerosol effects on deep convection: the propagation of aerosol perturbations through convective cloud microphysics. *Atmos. Chem. Phys.*, **19**, 2601–2627, https://doi.org/10.5194/acp-19-2601-2019.

Herman, J., A. Cede, E. Spinei, G. Mount, M. Tzortziou, and N. Abuhassan, 2009: NO2 column amounts from ground-based Pandora and MFDOAS spectrometers using the direct-sun DOAS technique: Intercomparisons and application to OMI validation. J. Geophys. Res.: Atm., **114**(D13). https://doi.org/10.1029/2009JD011848

Hernandez-Deckers, D., T. Matsui, and A. M. Fridlind, 2022: Updraft dynamics and microphysics: on the added value of the cumulus thermal reference frame in simulations of aerosol-deep convection interactions, *Atmos. Chem. Phys*., **22**, 711–724, https://doi.org/10.5194/acp-22-711-2022.

Hersbach, H., et al. 2020: The ERA5 global reanalysis. *Quart. J. Roy. Meteor. Soc.*, **146**(730), https://doi.org/10.1002/qj.3803.

Hu, J, D. Rosenfeld, A. Ryzhkov, D. Zrnic, E. Williams, P. Zhang, J. C. Snyder, R. Zhang, and R. Weitz, 2019: Polarimetric radar convective cell tracking reveals large sensitivity of cloud precipitation and electrification properties to CCN. *J. Geophys. Res. – Atmos*. **124**(22): 12,194– 12,205, https://doi.org/10.1029/2019JD030857

Igel, A. L., and S. C. van den Heever, 2021: Invigoration or enervation of convective clouds by aerosols? *Geophys. Res. Lett.*, **48**(16), e2021GL093804, https://doi.org/10.1029/2021GL093804

Jensen, M. P., L. Judd, P. Kollias, J. Sullivan, R. Nadkarni, C. Kuang, G. McFarquhar, H. Powers and J. Flynn, 2022: A succession of cloud, precipitation, aerosol and air quality field experiments in the coastal urban environment. *Bull. Amer. Meteor. Soc*., https://doi.org/10.1175/BAMS-D-21-0104.1.

Jensen M. P., J. H. Flynn III, P. Kollias, C. Kuang, G. McFarquhar, H. Powers, S. Brooks, E. Bruning, D. Collins, S. M. Collis, J. Fan, A. M. Fridlind, S. E. Giangrande, R. Griffin, J. Hu, R. C. Jackson, M. Kumjian, T. Logan, T. Matsui, C. J. Nowotarski, M. Oue, A. D. Rapp, D. Rosenfeld, A. Ryzhkov, R. J. Sheesley, J. Snyder, P. Stier, S. Usenko, S. C. van den Heever, M. van Lier-Walqui, A. Varble, Y. Wang, A. Aiken, M. Deng, D. Dexheimer, M. Dubey, Y. Feng, V. Ghate, K. Johnson, D. Wang, M. Zawadowicz, and A.

Accepted for publication in *Bulletin of the American Meteorological Society*. DOI 10.1175/BAMS-D-23-0331.1.

Zhou. 2023. Tracking Aerosol Convection Interactions Experiment (TRACER) Field Campaign Report. Ed. by Robert Stafford, ARM user facility. DOE/SC-ARM-23-038. https://doi.org/10.2172/2202672.

Judd, L. M., J. A. Al-Saadi, S. J. Janz, M. G. Kowalewski, R. B. Pierce, J. J. Szykman, L. C. Valin, R. Swap, A. Cede, M. Mueller, M. Tiefengraber, N. Abuhassan, and D. Williams, 2019: Evaluating the impact of spatial resolution on tropospheric NO2 column comparisons within urban areas using high-resolution airborne data. *Atmos. Meas. Tech*., **12**(11), 6091–6111. https://doi.org/10.5194/amt-12-6091-2019

Judd, L.A., J. T. Sullivan, B. Lefer, J. Haynes, M. P. Jensen, and R. Nadkarni, 2021: TRACER-AQ Science Plan: An Interagency Cooperative Air Quality Field Study in the Houston, TX Metropolitan Region. https://www-air.larc.nasa.gov/missions/tracer-aq/docs/TRACERAQ_SciencePlan_v1.pdf

Kasparoglu, S., L. Cia, N. Meskhidze and M. D. Petters, 2024a: Evolution of refractory black carbon mixing state in an urban environment. *Atmos. Env.*, **333**, https://doi.org/10.1016/j.atmosenv.2024.120651.

Kasparoglu, S., N. Meskhidze, and M. D. Petters, 2024b: Aerosol mixing state, new particle formation, and cloud droplet number concentration in an urban environment. *Sci. Tot. Env.*, **951**, https://doi.org/10.1016/j.scitotenv.2024.175307.

Klein, P., E. Smith, T. Wagner, J. Gibbs, T. Bell, J. Gebauer, M. Spencer, and M. Carney, 2023: TRACER-Coastal Urban Boundary-Layer Interactions with Convection (CUBIC) Field Campaign Report. U.S. Department of Energy, ARM user facility, Richland, Washington. DOE/SC-ARM-23-027, https://www.arm.gov/publications/programdocs/doe-sc-arm-23-027.pdf

Kollias, P., E. E. Clothiaux, T. P. Ackerman, B. A. Albrecht, K. B. Widener, K. P. Moran, E. P. Luke, K. L. Johnson, N. Bharwadaj, J. B. Mead, M. A. Miller, J. Verlinde, R. T. Marchand, and G. G. Mace, 2016: Development and applications of ARM millimeter-wavelength cloud radars, *AMS Meteorol. Mono*., **57**, 17.1-17.19, https://doi.org/10.1175/AMSMONOGRAPHS-D-15-0037.1.

Kollias, P., E. E. Clothiaux, B. A. Albrecht, M. A. Miller, K. P. Moran, and K. L. Johnson, 2005: The Atmospheric Radiation Measurement program cloud profiling radars: An

Accepted for publication in *Bulletin of the American Meteorological Society*. DOI 10.1175/BAMS-D-23-0331.1.

evaluation of signal processing and sampling strategies, *J. Atmos. Ocean. Tech*., **22**, 930–948, https://doi.org/10.1175/JTECH1749.1.

Kollias, P., E. Luke and K. Lamer, 2023: Experiment of Sea Breeze Convection, Aerosols, Precipitation and Environment (ESCAPE) C-band Radar Deployment Field Campaign Report. U.S. Department of Energy, Atmospheric Radiation Measurement user facility, Richland, Washington. DOE/SC-ARM-23-039.

Kollias, P., E. P. Luke, K. Tuftedal, M. Dubois and E. J. Knapp, 2022a: Agile Weather Observations using a Dual-Polarization X-band Phased Array Radar, *2022 IEEE Radar Conference (RadarConf22)*, New York City, NY, USA, 2022, pp. 1-6, https://doi.org/10.1109/RadarConf2248738.2022.9764308.

Kollias, P., G. M. McFarquhar, M. Oue, S. van den Heever, T. Logan, E. Bruning, K. Lombardo, M. R. Kumjian, Z. Lebo, R. Shaw, G. Roberts, P. DeMott, and 42 additional co-authors, 2024: Experiment of Sea Breeze Convection, Aerosols, Precipitation and Environment (ESCAPE). *Bull. Amer. Meteor. Soc*., https://doi.org/10.1175/BAMS-D-23-0014.1

Kollias, P., R. Palmer, D. Bodine., T. Adachi, H. Bluestein, J. Y. Cho., C. Griffin, J. Houser, P. E. Kirstetter, M. R. Kumjian, J. M. Kurdzo, W. C. Lee, E. P. Luke, S. Nesbitt, M. Oue, A. Shapiro, A. Rowe, J. Salazar, R. Tanamachi, K. S. Tuftedal, X. Wang, S. Zrnic and B. P. Treserras, 2022b: Science applications of phased array radars. *Bull. Amerr. Meteor. Soc.*, **103**(10), E2370-E2390, https://doi.org/10.1175/BAMS-D-21-0173.1.

Kollias, P., J. S. Sodhi, M. Oue, N. Allwayin, E. P. Luke, K. Lamer, B. P. Treserras and A. Battaglia, 2025: High Spatiotemporal Resolution Observations of Deep Convective Motions using Multisensor Agile Adaptive Sampling. Submitted to *Atmos. Chem. Phys*.

Komhyr, W. D., 1986: Operations handbook-ozone measurements to 40-km altitude with Model 4A Electrochemical Concentration Cell (ECC) ozonesondes (used with 1680-MHz radiosondes). NOAA Tech. Memo. ERL ARL-149, Boulder, CO: Air Resour. Lab.

Kowalewski, M. G., and S. J. Janz, 2014: Remote sensing capabilities of the GeoCAPE Airborne Simulator. *Earth Observing Systems XIX*, **9218**, 496–507. https://doi.org/10.1117/12.2062058

Accepted for publication in *Bulletin of the American Meteorological Society*. DOI 10.1175/BAMS-D-23-0331.1.

Kuang, C., P. H. McMurry, and A. V. McCormick, 2009: Determination of cloud condensation nuclei production from measured new particle formation events. *Geophys Res Lett*, **36**, https://doi.org/10.1029/2009gl037584.

Kumar, J., Y. Li, G. S. Chelluboyina, B. J. Sumlin, J. V. Puthussery, T. S. Kapoor, and R. K Chakrabarty, 2024: Correcting filter-based aerosol light absorption measurement biases in a coastal urban-industrial region. *Aerosol Sci. Tech*., **58**(10), 1129-1141.

Kumjian, M. R., A. P. Khain, N. Benmoshe, E. Illotoviz, A. V. Ryzhkov, and V. T. J. Phillips, 2014: The anatomy and physics of ZDR columns: Investigating a polarimetric radar signature with a spectral bin microphysical model. *J. Appl. Meteor. Clim*., **53**(7), 1820-1843. https://doi.org/10.1175/JAMC-D-13-0354.1.

Lamer, K., E. P. Luke, B. Walsh Jr., S. Andrade, Z. Mages, Z. Zhu, E. Leghart, B. P. Treserras, A. Emrick, P. Kollias, and A. Vogelmann, 2022: Going mobile to address emerging climate equity needs in the heterogeneous urban environment. *Bull. Amer. Meteor. Soc.*, **103**(9), pp. E2069-E2080.

Lamer, K., P. Kollias, E. P. Luke, B. P. Treserras, M. Oue, and B. Dolan, 2023: Multisensor Agile Adaptive Sampling (MAAS): A Methodology to Collect Radar Observations of Convective Cell Life Cycle. *J. Atmos. Oceanic Technol.*, **40**, 1509–1522, https://doi.org/10.1175/JTECH-D-23-0043.1.

Lamer, K, Z. Mages, B. Puigdomènech Treserras, P. Walter, Z. Zhu, A. D. Rapp, C. J. Nowotarski, S. D. Brooks, J. Flynn, M. Sharma, P. Klein, M. Spencer, E. Smith, J. Gebauer, T. Bell, L. Bunting, T. Griggs, T. J. Wagner, and K. McKeown, 2024: Spatially distributed atmospheric boundary layer properties in Houston–A value-added observational dataset. *Scientific Data,* **11**, 661. https://doi.org/10.1038/s41597-024-03477-9.

Lappin, F., G. de Boer, P. Klein, J. Hamilton, M. Spencer, R. Calmer, A. Segales, M. Rhodes, T. Bell, J. Buchli, K. Britt, E. Asher, I. Medina, B. Butterworth, L. Otterstatter, M. Ritsch, B. Puxley, A. Miller, A. Jordan, C. Gomez-Faulk, E. Smith, S. Borenstein, T. Thornberry, B. Argrow, and E. Pillar-Little, 2024: Data collected using small uncrewed aircraft system during the TRacking Aerosol Convection Interactions ExpeRiment (TRACER), *Earth Sys. Sci. Data*, **16**, 2525–2541. https://doi.org/10.5194/essd-16-2525-2024

Accepted for publication in *Bulletin of the American Meteorological Society.* DOI 10.1175/BAMS-D-23-0331.1.

Li, W., Y, Wang, X. Liu, E. Soleimanian, T. Griggs, J. Flynn and P. Walter, 2023: Understanding offshore high-ozone events during TRACER-AQ 2021 in Houston: Insights from WRF-CAMx photochemical modeling. *Atmos. Chem. Phys.*, **23**, 13685-13699. https://doi.org/10.5194/acp-23-13685-2023.

Liu, X., Y. Wang, S. Wasti, E. Li, E. Soleimanian, J. Flynn, T. Griggs, S. Alvarez, J. T. Sullivan, M. Roots, L. Twigg, G. Gronoff, T. Berkoff, P. Walter, M. Estes, J. W. Hair, T. Shingler, A. J. Scarino, M. Fenn, and L. Judd, 2023: Evaluating WRF-GC v2.0 predictions of boundary layer height and vertical ozone profile during the 2021 TRACER-AQ campaign in Houston, Texas. *Geosci. Model Dev.*, **16**(18), 5493–5514. https://doi.org/10.5194/gmd-16-5493-2023

Logan, T., E. Bruning, K. Brunner, and J. Souza, 2023: Houston Lightning Mapping Array (HLMA) Flash-level data. Version 1.0. UCAR/NCAR - Earth Observing Laboratory, doi: 10.26023/GBKS-E7VT-HS11.

Mages, Z., P. Kollias, B. P. Treserras, P. Borque, and M. Oue, 2024: Shallow cloud variability in Houston, Texas during the ESCAPE and TRACER field experiments, EGUsphere [preprint], https://doi.org/10.5194/egusphere-2024-2984.

Marinescu, P. J., S. C. van den Heever, M. Heikenfeld, A. I. Barrett, C. Barthlott, C. Hoose, J. Fan, A. M. Fridlind, T. Matsui, A. K. Miltenberger, P. Stier, B. Vie, B. A. White, and Y. Zhang, 2021: Impacts of Varying Concentrations of Cloud Condensation Nuclei on Deep Convective Cloud Updrafts–A Multimodel Assessment. *J. Atmos. Sci.* **78**(4): 1147–1172, https://doi.org/10.1175/JAS-D-20-0200.1

Mather, J. H. and J. W. Voyles, 2013: The ARM Climate Research Facility: A Review of Structure and Capabilities. *Bull. Amer. Meteor. Soc.*, **94**(3), 377-392. https://doi.org/10.1175/BAMS-D-11-00218.1.

Matsui, T., D. Hernandez-Deckers, S. E. Giangrande, T. S. Biscaro, A. Fridlind, and S. Braun, 2024: A thermal-driven graupel generation process to explain dry-season convective vigor over the Amazon, *Atmos. Chem. Phys.*, **24**, 10793–10814, https://doi.org/10.5194/acp-24-10793-2024.

Accepted for publication in *Bulletin of the American Meteorological Society.* DOI 10.1175/BAMS-D-23-0331.1.

McKeown, K. E., K. Lombardo, and M. R. Kumjian, 2025: Environmental Characteristics Supporting Warm-Season Coastal Convection Initiation Near Houston, Texas. *Wea. Forecasting*, Accepted.

Miller, M. A., K. Nitschke, T. P. Ackerman, W. Ferrell, N. Hickmon, and M. Ivey, 2016: The atmospheric radiation measurement mobile facility, The atmospheric radiation measurement (ARM) program: AMS monograph, the first 20 years of arm. American Meteorological Society, 57, 9. https://doi.org/10.1175/AMSMONOGRAPHS-D-15-0051.1

Morrison, H., J. A. Curry, and V. I. Khvorostyanov, 2005: A new double-moment microphysics parameterization for application in cloud and climate models. Part I: Description, *J. Atmos. Sci.,* **62**, 1665–1677, https://doi.org/10.1175/Jas3446.1

Morrison, H., G. Thompson, and V. Tatarskii, 2009: Impact of Cloud Microphysics on the Development of Trailing Stratiform Precipitation in a Simulated Squall Line: Comparison of One- and Two-Moment Schemes, *Mon. Weather Rev*., **137**, 991–1007, https://doi.org/10.1175/2008mwr2556.1.

Morrison, H., and J. Milbrandt, 2011: Comparison of Two-Moment Bulk Microphysics Schemes in Idealized Supercell Thunderstorm Simulations, *Mon. Weather Rev*., **139**, 1103–1130, https://doi.org/10.1175/2010mwr3433.1.

Müller, D., C. A. Hostetler, R. A. Ferrare, S. P. Burton, E. Chemyakin, A. Kolgotin, J. W. Hair, A. L. Cook, D. B. Harper, R. R. Rogers, R. W. Hare, C. S. Cleckner, M. D. Obland, J. Tomlinson, L. K. Berg, and B. Schmid, 2014: Airborne Multiwavelength High Spectral Resolution Lidar (HSRL-2) observations during TCAP 2012: Vertical profiles of optical and microphysical properties of a smoke/urban haze plume over the northeastern coast of the US. *Atmos. Meas. Tech*., **7**(10), 3487–3496. https://doi.org/10.5194/amt-7-3487-2014

Nowlan, C. R., X. Liu, S. J. Janz, M. G. Kowalewski, K. Chance, M. B. Follette-Cook, A. Fried, G. González Abad, J. R. Herman, L. M. Judd, H.-A. Kwon, C. P. Loughner, K. E. Pickering, D. Richter, E. Spinei, J. Walega, P. Weibring, and A. J. Weinheimer, 2018: Nitrogen dioxide and formaldehyde measurements from the GEOstationary Coastal and Air Pollution Events (GEO-CAPE) Airborne Simulator over Houston, Texas, *Atmos. Meas. Tech.*, **11**, 5941–5964, https://doi.org/10.5194/amt-11-5941-2018.

Accepted for publication in *Bulletin of the American Meteorological Society.* DOI 10.1175/BAMS-D-23-0331.1.

Oktem, R. Stereo Reconstructed Point Cloud of Cloud Points (PCCP) (PCCP), 2021-10-01 to 2022-09-28, ARM Mobile Facility (HOU), Houston, TX; Supplemental Facility 5 for stereo cameras (S5). Atmospheric Radiation Measurement (ARM) User Facility. https://doi.org/10.5439/1971200

Olaguer, E.P., C.E. Kolb, B. Lefer, B. Rappenglueck, R.Y. Zhang, and J.P. Pinto. 2014. Overview of the SHARP campaign: Motivation, design, and major outcomes. *J. Geophys. Res. Atmos.* 119(5):2597–610. https://doi.org/10.1002/2013jd019730.

Patil et al. (in prep)

Parrish, D. D., D. T. Allen, T. S. Bates, M. Estes, F. C. Fehsenfeld, G. Feingold, R. Ferrare, R. M. Hardesty, J. F. Meagher, J. W. Nielsen-Gammon, R. B. Peirce, T. B. Ryerson, J. H. Seinfeld and E. J. Williams, 2009: Overview of the Second Texas Air Quality Study (TexAQS II) and the Gulf of Mexico Atmospheric Composition and Climate Study (GoMACCS), *J. Geophys. Res.*, **114**, D00F13, https://doi.org/10.1029/2009JD011842

Pazmany, A. L., J. B, Mead, H. B. Bluestein, J. C. Snyder, and J. B. Houser, 2013: A mobile rapid Rapid-scanning X-band Polarimetric (RaXPol) Doppler radar system. *J. Atmos. Oceanic Tech.*, **30**(7), 1398-1413. https://doi.org/10.1175/JTECH-D-12-00166.1.

Pehl, J., G.M. McFarquhar, J. Snyder and J. Furtado, 2025: Exploring impacts of differing aerosol environments on radar signatures of deep convection near Houston, TX using a bulk statistical framework. *J. Atmos. Sci.*, **82**(4), 749-774. https://doi.org/10.1175/JAS-D-24-0008.1.

Peters, J. M., D. R. Chavas, C.-Y. Su, H. Morrison, and B. E. Coffer, 2023: An analytic formula for entraining CAPE in midlatitude storm environments. *J. Atmos. Sci.*, **80**(9), 2165-2186. https://doi.org/10.1175/JAS-D-23-0003.1.

Peters-Lidard, C.D., E. M. Kemp, T. Matsui, J. A. Santanello, Jr., S. V., Kumar, J. P. Jacob, T. Clune, W.-K. Tao, M. Chin, A. Hou, J. L. Case,, D. Kim, K.-M. Kim, W. Lau, Y. Liu, J.-J. Shi, D. Starr, Q. Tan,, Z. Tao, B. F. Zaitchik, B. Zavodsky, S. Q. Zhang, M. Zupanski, 2015: Integrated modeling of aerosol, cloud, precipitation and land processes at satellite-resolved scales, *Environmental Modelling & Software*, **67**, 149–159, http://dx.doi.org/10.1016/j.envsoft.2015.01.007

Accepted for publication in *Bulletin of the American Meteorological Society*. DOI 10.1175/BAMS-D-23-0331.1.

Rahman, K., G. Rios, H. Gamarro, O. Addasi, J. C. Pena, J. Gonzalez-Cruz, R. Bornstein and P. Ramamurthy, 2024: The boundary layer characteristics of coastal urban environments. *Theor. Appl. Climatol.,* **155**, 6931–6948. https://doi.org/10.1007/s00704-024-05036-z

Rapp, A. D., S. D. Brooks, C. J. Nowotarski, M. Sharma, S. A. Thompson, B. Chen, B. H. Matthews, M. Etten-Bohm, E. R. Nielsen and R. Li, 2024: TAMU TRACER: Targeted Mobile Measurements to Isolate the Impacts of Aerosols and Meteorology on Deep Convection. *Bull. Amer. Meteor. Soc*., https://doi.org/10.1175/BAMS-D-23-0218.1.

Ren, J., L. Chen, T. Fan, J. Liu, S. Jiang, and F. Zhang, 2021: The NPF Effect on CCN Number Concentrations: A Review and Re-Evaluation of Observations From 35 Sites Worldwide. *Geophys Res Lett*, 48, e2021GL095190, https://doi.org/10.1029/2021GL095190

Romps, D. M., K. Latimer, Q. Zhu, T. Jurkat-Witschas, C. Mahnke, T. Prabhakaran, R. Weigel and M. Weindisch, 2023: Air pollution unable to intensify storms via warm-phase invigoration. *J. Geophys. Res.*, 50(2), https://doi.org/10.1029/2022GL100409.

Rosenfeld, D., Y. Zheng, E. Hashimshoni, and M. O. Andreae, 2016: Satellite retrieval of cloud condensation nuclei concentrations by using clouds as CCN. Proc. Nat. Academ. Sci., 113 (21), 5828-5834. https://doi.org/10.1073/pnas.1514044113.

Saleeby, S. M., S. C. van den Heever, P. J. Marinescu, M. Oue, A. I. Barrett, C. Barthlott, R. Cherian, J. Fan, A. M. Fridlind, M. Heikenfeld, C. Hoose, T. Matsui, A. K. Miltenberger, J. Quaas, J. Shpund, P. Stier, B. Vie, B. A. White, Y. Zhang, 2025: Model intercomparison of the impacts of varying cloud droplet nucleating aerosols on the lifecycle and microphysics of isolated deep convection. *J. Atmos. Sci*., In review.

Sharma, M., A. D. Rapp, C. J. Nowotarski, and S. D. Brooks, 2024: Observed variability in convective cell characteristics and near-storm environments across the sea and bay-breeze fronts in southeast Texas. *Mon. Weather Rev.,* **152***,* 2419–2441, https://doi.org/10.1175/MWR-D-23-0243.1.

Shrestha, S., S. Yoon, S. L. Alvarez, Y. Wang, J. H. Flynn, S. Usenko, and R. J. Sheesley, 2023: Emission Ratios and Diurnal Variability of Volatile Organic Compounds and Influence of Industrial Emissions in Two Texas Cities. *Atmosphere*, **14**(6), 1006. https://doi.org/10.3390/atmos14061006

Accepted for publication in *Bulletin of the American Meteorological Society.* DOI 10.1175/BAMS-D-23-0331.1.

Smit, H., and A. Thompson, 2021: Ozonesonde Measurement Principles and Best Operational Practices: ASOPOS 2.0 (Assessment of Standard Operating Procedures for Ozonesondes), WMO. World Meteorological Organization, GAW Report, 268, 173.

Smith, J. N., K. F. Moore, P. H. McMurry, and F. L. Eisele, 2004: Atmospheric Measurements of Sub-20 nm Diameter Particle Chemical Composition by Thermal Desorption Chemical Ionization Mass Spectrometry. *Aerosol Sci. Tech.*, ***38***(2), 100–110. https://doi.org/10.1080/02786820490249036

Sokolowsky, G. A., S. W. Freeman, W. K. Jones, J. Kukulies, F. Senf, P. J. Marinescu, M. Heikenfeld, K. N. Brunner, E. C. Bruning, S. M. Collis, R. C. Jackson, G. R. Leung, N. Pfeifer, B. A. Raut, S. M. Saleeby, P. Stier, and S. C. van den Heever, 2024: tobac v1.5: introducing fast 3D tracking, splits and mergers, and other enhancements for identifying and analysing meteorological phenomena. *Geosci. Model Dev.*, **17**, 5309–5330, https://doi.org/10.5194/gmd-17-5309-2024.

Soleimanian, E., Y. Wang., W. Li, X. Liu, T. Griggs, J. Flynn, P. J. Walter, and M. J. Estes, 2023: Understanding ozone episodes during the TRACER-AQ campaign in Houston, Texas: The role of transport and ozone production sensitivity to precursors. *Science of The Total Environment*, 900, 165881. https://doi.org/10.1016/j.scitotenv.2023.165881

Storm, M. R., Klein, P. M., Smith, E. N., Wagner, T., 2025: Spatial heterogeneity of planetary boundary layer height within a coastal-urban environment. In preparation.

Subba T., M. P. Jensen, M. Deng, S. E. Giangrande, M. C. Harvey, A. Singh, D. Wang, M. Zawadowicz and C. Kuang, 2025: Implications of sea breeze circulation on boundary layer aerosols in the southern coastal Texas region. EGUsphere [preprint], https://doi.org/10.5194/egusphere-2025-2659, 2025.

Sullivan, J., J. Hair, T. Shingler, R. Ferrare, M. Fenn, T. Berkoff, G. Gronoff, M. Roots, T. Nyugen, L. Twigg, J. Flynn, T. Griggs, P. Walter, T. Hanisco, A. Kotsakis, E. J. Welton, and L. Judd, 2023: Advances in Characterizing Pollution Transport with Ground-Based and Airborne Profilers: Case Studies Within Houston, TX. In J. T. Sullivan, T. Leblanc, S. Tucker, B. Demoz, E. Eloranta, C. Hostetler, S. Ishii, L. Mona, F. Moshary, A. Papayannis, & K. Rupavatharam (Eds.), Proceedings of the 30th International Laser Radar Conference (pp. 765–772). Springer International Publishing. https://doi.org/10.1007/978-3-031-37818-8_98

Accepted for publication in *Bulletin of the American Meteorological Society.* DOI 10.1175/BAMS-D-23-0331.1.

Sullivan, J. T., T. J. McGee, T. Leblanc, G. K. Sumnicht, and L. W. Twigg, 2015: Optimization of the GSFC TROPOZ DIAL retrieval using synthetic lidar returns and ozonesondes – Part 1: Algorithm validation. *Atmos. Meas. Tech*., **8**(10), 4133–4143. https://doi.org/10.5194/amt-8-4133-2015

Toon, O. B., H. Maring, J. Dibb, R. Ferrare, D. J. Jacob, E. J. Jensen, Z. J. Luo, G. G> Mace, L. L. Pan, L. Pfister, K. H. Rosenlof, J. Redemann, J. S. Reid, H. B. Singh, A. M. Thompson, R. Yokelson, P. Minnis, G. Chen, K. W> Jucks, and A. Pszenny, 2016: Planning, implementation, and scientific goals of Emissions and Atmospheric Composition, Clouds and Climate Coupling by Regional Surveys (SEAC4RS) field mission. *J. Geophys. Res*., **121**(9), 4967-5009. https://doi.org/10.1002/2015JD024297.

Tuftedal, K. S., B. Puigdomènech Treserras, M. Oue, and P. Kollias, 2024: Shallow- and deep-convection characteristics in the greater Houston, Texas, area using cell tracking methodology. *Atmos. Chem. Phys*., **24** (9), 5637-5657. https://doi.org/10.5194/acp-24-5637-2024.

Uin, J., A. C. Aiken, M. K. Dubey, C. Kuang, M. Pekour, C. Salwen, A. J. Sedlacek, G. Senum, S. Smith, J. Wang, T. B. Watson and S. R. Springston, 2019: Atmospheric Radiation Measurement (ARM) Aerosol Observing Systems (AOS) for surface-based in situ atmospheric aerosol and trace gas measurements. *J. Atmos. Oceanic Tech*., **36**(12), 2429-2447. https://doi.org/10.1175/JTECH-D-19-0077.1

U.S. Census Bureau, "RACE," Decennial Census, DEC Redistricting Data (PL 94-171), Table P1, accessed on July 1, 2025, https://data.census.gov/table/DECENNIALPL2020.P1?t=Populations+and+People&g=050XX00US48039,48071,48157,48167,48201,48291,48339,48473.

van den Heever, S.C., and Coauthors, 2017: Aerosol-Cloud-Precipitation-Climate (ACPC) initiative: Deep Convective Cloud Group roadmap. ACPC Rep., 13 pp., http://acpcinitiative.org/Docs/ACPC_DCC_Roadmap_171019.pdf.

van den Heever, S. C., P. J. Marinescu, M. Heikenfeld, B. White, A. Fridlind, P. Stier, M. Andreae, A. Barrett, C. Barthlott, R. Cherian, J. Fan, C. Hoose, T. Matsui, A. Miltenberger, J. Quaas, D. Rosenfeld, J. Shpund, B. Vie, Y. Zhang, and Stephen M.

Accepted for publication in *Bulletin of the American Meteorological Society*. DOI 10.1175/BAMS-D-23-0331.1.

Saleeby 2025: A model intercomparison project exploring aerosol impacts on deep convective clouds. *Bull. Amer. Met. Soc.* Submitted.

van Lier-Walqui M., A.M. Fridlind, A.S. Ackerman, S. Collis, J. Helmus, D.R. MacGorman, K. North, P. Kollias, and D.J. Posselt, 2016: On polarimetric radar signatures of deep convection for model evaluation: Columns of specific differential phase observed during MC3E. *Mon. Wea. Rev.*, **144**(2), https://doi.org/10.1175/mwr-d-15-0100.1.

Varble, A. C., A. L. Igel, H, Morrison, W. W. Grabowski and Z. J. Lebo, 2024: Opinion: A critical evaluation of the evidence for aerosol invigoration of deep convection. *Atmos. Chem. Phys.*, **23**(21), 13791-13808. https://doi.org/10.5194/acp-23-13791-2023.

Voisin, D., J. N. Smith, H. Sakurai, P. H. McMurry, and F. L. Eisele, 2003: Thermal Desorption Chemical Ionization Mass Spectrometer for Ultrafine Particle Chemical Composition. *Aerosol Sci. Tech.*, ***37***(6), 471–475. https://doi.org/10.1080/02786820300959

Wang, D., M. P. Jensen, D. Taylor, G. Kowalski, M. Hogan, B. M. Wittemann, A. Rakotoarivony, S. E. Giangrande, and J. Minnie Park, 2022: Linking synoptic patterns to cloud properties and local circulations over southeastern Texas. *J. Geophys. Res*., **127** (5), https://doi.org/10.1029/2021JD035920

Wang, D., R. W. Kobrosly, T. Subba, T. Zhang. S. C. van den Heever, M. P. Jensen and S. Gupta, 2025: Causal Analysis of Aerosol Impacts on Isolated Deep Convection: Findings from TRACER. *Atmos. Chem. Phys.,* in revision.

Wang, D., E. C. Melvin, N. Smith, M. P. Jensen, S. Gupta, A. Abdullah-Smoot, N. Pszeniczny, and T. Hahn, 2024: TRACER perspectives on gulf-breeze and bay-breeze circulations and coastal convection. *Mon. Wea. Rev*., **152**(10), 2207-2228. https://doi.org/10.1175/MWR-D-23-0292.1

Wagner, T. J., Klein, P. M., Turner, D. D., 2019: A new generation of ground-based mobile platforms for active and passive profiling of the boundary layer. *Bull. Am. Meteor. Soc.*, 100(1), 137-153, https://doi.org/10.1175/BAMS-D-17-0165.1.

Welton, E. J., Campbell, J. R., Spinhirne, J. D., & Iii, V. S. S. (2001). Global monitoring of clouds and aerosols using a network of micropulse lidar systems. Lidar Remote Sensing for Industry and Environment Monitoring, 4153, 151–158. https://doi.org/10.1117/12.417040

Accepted for publication in *Bulletin of the American Meteorological Society.* DOI 10.1175/BAMS-D-23-0331.1.

Yoon, S., S. M. Ortiz, A. E. Clark, T. E. Barrett, S. Usenko, R. M. Duvall, L. Hildebrandt Ruiz, J. K. Bean, C. B. Faxon, J. H. Flynn, B. L. Lefer, Y. J. Leong, R. J. Griffin, and R. J. Sheesley, 2021: Apportioned primary and secondary organic aerosol during pollution events of DISCOVER-AQ Houston. *Atmos. Environ*. **244**. https://doi.org/10.1016/j.atmosenv.2020.117954

Young, R. D., W. Carrion, R. Ganoe, D. Pliutau, G. Gronoff, T. Berkoff, and S. Kuang, 2017: Langley mobile ozone lidar: Ozone and aerosol atmospheric profiling for air quality research. *Applied Optics*, **56**(3), 721–730. https://doi.org/10.1364/AO.56.000721

Zhang, Y., J. Fan, Z. Li, and D. Rosenfeld, 2021.: Impacts of cloud microphysics parameterizations on simulated aerosol–cloud interactions for deep convective clouds over Houston, *Atmos. Chem. Phys*., **21**, 2363–2381, https://doi.org/10.5194/acp-21-2363-2021.

Zoogman, P., X. Liu, R. M. Suleiman, W. F. Pennington, D. E. Flittner, J. A. Al-Saadi, B. B. Hilton, D. K. Nicks, M. J. Newchurch, J. L. Carr, S. J. Janz, M. R. Andraschko, A. Arola, B. D. Baker, B. P. Canova, C. Chan Miller, R. C. Cohen, J. E. Davis, M. E. Dussault, D. P. Edwards, J. Fishman, A. Ghulam, G. González Abad, M. Grutter, J. R. Herman, J. Houck, D. J. Jacob, J. Joiner, B. J. Kerridge, J. Kim, N. A. Krotkov, L. Lamsal, C. Li, A. Lindfors, R. V. Martin, C. T. McElroy, C. McLinden, V. Natraj, D. O. Neil, C. R. Nowlan, E. J. O′ Sullivan, P. I. Palmer, R. B. Pierce, M. R. Pippin, A. Saiz-Lopez, R. J. D. Spurr, J. J. Szykman, O. Torres, J. P. Veefkind, B. Veihelmann, H. Wang, J. Wang, and K. Chance, 2017: Tropospheric emissions: Monitoring of pollution (TEMPO), *Journal of Quantitative Spectroscopy and Radiative Transfer*, **186**, 17–39, https://doi.org/10.1016/j.jqsrt.2016.05.008.

Accepted for publication in *Bulletin of the American Meteorological Society*. DOI 10.1175/BAMS-D-23-0331.1.